

Light-quarks Yukawa and new physics in exclusive high- p_T Higgs + jet(b-jet) events

Jonathan Cohen,^{1,*} Shaouly Bar-Shalom,^{1,†} Gad Eilam,^{1,‡} and Amarjit Soni^{2,§}

¹*Physics Department, Technion-Institute of Technology, Haifa 32000, Israel*

²*Physics Department, Brookhaven National Laboratory, Upton, NY 11973, USA*

(Dated: May 27, 2022)

We suggest that the exclusive Higgs + light (or b)-jet production at the LHC, $pp \rightarrow h + j(j_b)$, is a rather sensitive probe of the light-quarks Yukawa couplings and of other forms of new physics (NP) in the Higgs-gluon hgg and quark-gluon qqg interactions. We study the Higgs p_T -distribution in $pp \rightarrow h + j(j_b) \rightarrow \gamma\gamma + j(j_b)$, i.e., in $h + j(j_b)$ production followed by the Higgs decay $h \rightarrow \gamma\gamma$, employing the (p_T -dependent) signal strength formalism to probe various types of NP which are relevant to these processes and which we parameterize either as scaled Standard Model (SM) couplings (the kappa-framework) and/or through new higher dimensional effective operators (the SMEFT framework). We find that the exclusive $h + j(j_b)$ production at the 13 TeV LHC is sensitive to various NP scenarios, with typical scales ranging from a few TeV to $\mathcal{O}(10)$ TeV, depending on the flavor, chirality and Lorentz structure of the underlying physics.

I. INTRODUCTION

The next runs of the LHC will be dedicated to two primary tasks: the search for new physics (NP) and the detailed scrutiny of the Higgs properties, which might shed light on NP specifically related to the origin of mass and flavor and to the observed hierarchy between the two disparate Planck and ElectroWeak (EW) scales. Indeed, the study of Higgs systems is in particular challenging, since it requires precision examination of some of its weakest couplings (within the SM) and measurements of highly non-trivial processes involving high jet multiplicities, large backgrounds and low detection efficiencies.

The s-channel Higgs production and its subsequent decays, $pp \rightarrow h \rightarrow ff$, which led to its discovery, are relatively inefficient for NP searches. In particular, if the NP scale, Λ , is of $\mathcal{O}(\text{TeV})$ and larger, then its effect in these processes is expected to be suppressed by at least $\sim m_h^2/\Lambda^2$, since most of these events come from the dominant gluon fusion s-channel production mechanism and are, therefore, clustered around $\sqrt{s} \simeq m_h$. However, in some fraction of the events, the Higgs recoils against one or more hard jets and, thus, carries a large p_T , which may play a key role in the hunt for NP and/or for background rejection in Higgs studies. Indeed, a key observable for Higgs boson events is the number of jets produced in the event. For that reason, and since the Higgs p_T distribution is sensitive to the production mechanism, there has recently been a growing interest, both experimentally [1–6] and theoretically [7–15], in the behavior of the Higgs p_T distribution in inclusive and exclusive Higgs production, where the Higgs carries a substantial fraction of transverse momentum (for earlier work see [16–19]). In particular, the Higgs p_T distribution in the

exclusive Higgs + jets production, $pp \rightarrow h + nj$, was one of the prime targets of the measurements performed recently by ATLAS and CMS [1–6].

In this paper we will thus focus on the exclusive Higgs + 1-jet production, $pp \rightarrow h + j$, where j stands for either a “light-jet” defined as any non-flavor tagged jet originating from a gluon or light-quarks $j = g, u, d, c, s$ (i.e., assuming them to be indistinguishable from the observational point of view) or a b -quark jet (j_b). It is interesting to note that there has been some hints in the LHC 8 TeV data for an excess in the $h + j$ channel [3, 9], although the statistics are still limited and the theoretical uncertainties are relatively large. Indeed, a significant effort has been dedicated in recent years, from the theory side, towards understanding and reducing the uncertainties pertaining to the Higgs+jet production cross-section at the LHC [7, 8, 10–13, 20–22], with special attention given to higher transverse momentum of the Higgs, where NP effects are expected to become more apparent. In particular, the high- p_T Higgs spectrum in $pp \rightarrow h + j(j_b)$ can be sensitive to various well motivated NP scenarios, such as supersymmetry [23–26], heavy top-partners [27], higher dimensional effective operators [28–32] and NP in Higgs-top quark and Higgs-gluon interactions in the so-called “kappa-framework”, where one assumes that the hgg and htt interactions are scaled by some factor with respect to the SM [33–36].

In general, there is a tree-level contribution to $pp \rightarrow h + j(j_b)$ in the SM from the hard processes $gq \rightarrow qh$, $g\bar{q} \rightarrow \bar{q}h$ and $q\bar{q} \rightarrow gh$ ($q = u, d, c, s, b$). The corresponding SM tree-level diagrams, which are depicted in Fig. 1, are proportional to the light-quarks Yukawa couplings, y_q , so that the SM tree-level contribution to the overall $pp \rightarrow h + j(j_b)$ cross-section is small (e.g., in the case of $pp \rightarrow h + c$, it is at the percent level). In particular, the squared matrix elements, summed and averaged over spins and colors, for these tree-level hard

*Electronic address: jcohen@tx.technion.ac.il

†Electronic address: shaouly@physics.technion.ac.il

‡Electronic address: eilam@physics.technion.ac.il

§Electronic address: adlersoni@gmail.com

processes are:

$$\sum \left| \mathcal{M}_{SM}^{q\bar{q} \rightarrow gh} \right|^2 = \frac{2g_s^2 y_q^2 m_h^4 + \hat{s}^2}{C_{qq} \hat{t} \hat{u}}, \quad (1)$$

$$\sum \left| \mathcal{M}_{SM}^{qg \rightarrow qh} \right|^2 = -\frac{C_{qq}}{C_{qq}} \sum \left| \mathcal{M}_{SM}^{q\bar{q} \rightarrow gh} \right|^2 (\hat{s} \leftrightarrow \hat{t}), \quad (2)$$

$$\sum \left| \mathcal{M}_{SM}^{\bar{q}g \rightarrow \bar{q}h} \right|^2 = -\frac{C_{qq}}{C_{qq}} \sum \left| \mathcal{M}_{SM}^{q\bar{q} \rightarrow gh} \right|^2 (\hat{s} \leftrightarrow \hat{u}), \quad (3)$$

where $\hat{s} = (p_1 + p_2)^2$, $\hat{t} = (p_1 + p_3)^2$ and $\hat{u} = (p_2 + p_3)^2$, defined for the process $q(-p_1) + \bar{q}(-p_2) \rightarrow h + g(p_3)$. Also, g_s is the strong coupling constant and $C_{qq} = N^2$, $C_{gg} = NV$ are the color average factors, where $V = N^2 - 1 = 8$ corresponds to the number of gluons in the adjoint representation of the SU(N) color group.

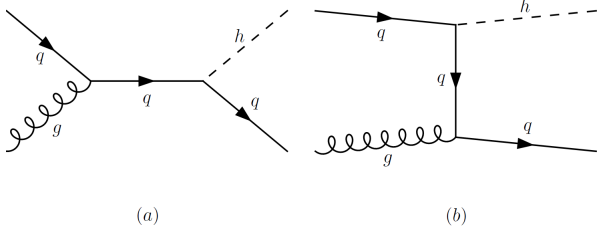


FIG. 1: The tree-level SM diagrams for $qg \rightarrow qh$, where $q = u, d, c, s, b$. The diagrams corresponding to $g\bar{q} \rightarrow h\bar{q}$ and $q\bar{q} \rightarrow gh$ can be obtained by crossing symmetry, see also text.

Thus, in the limit $y_q \rightarrow 0$, the dominant and leading order (LO) SM contribution to the Higgs + light-jet cross-section, $\sigma(pp \rightarrow h + j)$, arises from the 1-loop process $gg \rightarrow gh$, which is generated by 1-loop top-quark exchanges (and the subdominant b-quark loops), and can be parameterized by an effective Higgs-gluon ggh interaction Lagrangian:

$$\mathcal{L}_{eff}^{ggh} = C_g h G_{\mu\nu}^a G^{\mu\nu, a}, \quad (4)$$

where C_g is the SM Higgs-gluon 1-loop effective coupling, which at lowest order (i.e., at $\mathcal{O}(\alpha_s)$ and neglecting terms $\propto m_h^2/m_t^2$) is [16, 17]: $C_g = \alpha_s/(12\pi v)$, where $v = 246$ GeV is the Higgs vacuum expectation value (VEV).

The subprocesses $qg \rightarrow qh$, $g\bar{q} \rightarrow \bar{q}h$ and $q\bar{q} \rightarrow gh$ (which, as can be seen from Eqs. 1-3, are proportional to y_q^2 at tree-level) also receive a 1-loop contribution from the above ggh effective vertex (i.e., from the top-quark loops), which is, however, small compared to the $gg \rightarrow gh$ [16–19]. In particular, the $gg \rightarrow gh$ contribution to $\sigma(pp \rightarrow h + j)$ at the LHC is about an order of magnitude larger than the one from $qg \rightarrow qh$ and more than two orders of magnitude larger than the two other channels $g\bar{q} \rightarrow \bar{q}h$ and $q\bar{q} \rightarrow gh$.

The 1-loop (and LO for $y_q = 0$) SM differential hard cross-sections for $gg \rightarrow gh$, $qg \rightarrow qh$, $g\bar{q} \rightarrow \bar{q}h$ and $q\bar{q} \rightarrow gh$ (the corresponding SM diagrams for all channels are shown in Fig. 2), expressed in terms of the above effective ggh interaction and neglecting the light-quark masses,

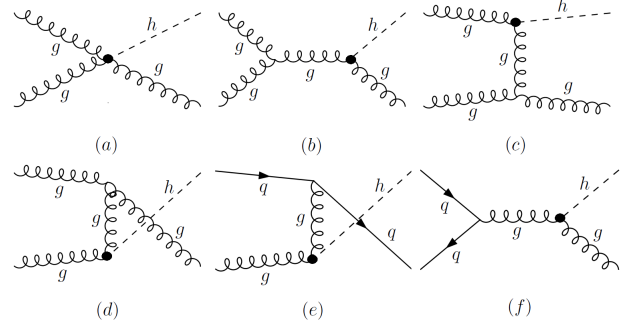


FIG. 2: The 1-loop SM diagrams for $gg \rightarrow gh$, $qg \rightarrow qh$ and $q\bar{q} \rightarrow gh$, in the effective Higgs-gluon description, where the loop-induced ggh and ggh vertices are represented by a heavy dot. See also text.

are given by [16, 17]:

$$\sum \left| \mathcal{M}_{SM}^{gg \rightarrow gh} \right|^2 \simeq \frac{96g_s^2 C_g^2 m_h^8 + \hat{s}^4 + \hat{t}^2 + \hat{u}^2}{C_{gg} \hat{s} \hat{t} \hat{u}}, \quad (5)$$

$$\sum \left| \mathcal{M}_{SM}^{q\bar{q} \rightarrow gh} \right|^2 \simeq \frac{16g_s^2 C_g^2 \hat{t}^2 + \hat{u}^2}{C_{qq} \hat{s}}, \quad (6)$$

$$\sum \left| \mathcal{M}_{SM}^{qg \rightarrow qh} \right|^2 \simeq -\frac{C_{qq}}{C_{qq}} \sum \left| \mathcal{M}_{SM}^{q\bar{q} \rightarrow gh} \right|^2 (\hat{s} \leftrightarrow \hat{t}), \quad (7)$$

$$\sum \left| \mathcal{M}_{SM}^{\bar{q}g \rightarrow \bar{q}h} \right|^2 \simeq -\frac{C_{qq}}{C_{qq}} \sum \left| \mathcal{M}_{SM}^{q\bar{q} \rightarrow gh} \right|^2 (\hat{s} \leftrightarrow \hat{u}), \quad (8)$$

where $C_{gg} = V^2 = 64$ and $\hat{s} = (p_1 + p_2)^2$, $\hat{t} = (p_1 + p_3)^2$, $\hat{u} = (p_2 + p_3)^2$, with momenta defined via $h \rightarrow g(p_1) + g(p_2) + g(p_3)$ for $gg \rightarrow gh$ and via $q(-p_1) + \bar{q}(-p_2) \rightarrow h + g(p_3)$ for $q\bar{q} \rightarrow gh$.

Turning now to the possible manifestation of NP in Higgs + jet production at the LHC, there are, in principle, two ways in which $pp \rightarrow h + j(j_b)$ can be modified:

- when the NP generates new interactions that are absent in the SM and that can potentially change the SM kinematic distributions in this process.
- when the NP comes in the form of scaled SM couplings, corresponding to the previously mentioned kappa-framework.

We will explore both types of NP effects in $pp \rightarrow h + j$ and $pp \rightarrow h + j_b$ and, in particular, focus on NP that modifies the light and b-quarks Yukawa couplings and/or the light and b-quarks interactions with the gluon, as well as the Higgs-gluon effective vertex in Eq. 4. Indeed, the Higgs mechanism of the SM implies that the fermion's Yukawa couplings are proportional to the ratio between their masses and the EW VEV, i.e., $y_f \propto m_f/v$. Thus, at least for the light fermions of the 1st and 2nd generations [where $m_f/v \sim \mathcal{O}(10^{-5})$ and $m_f/v \sim \mathcal{O}(10^{-4} - 10^{-3})$, respectively], any signal which can be associated with their Yukawa couplings would stand out as clear evidence for NP beyond the SM. The current experimental bounds on

the Yukawa couplings of light-quark's of the 1st and 2nd generations, y_u, y_d, y_s, y_c , coming from fits to the measured Higgs data, allow them to be as large as the b-quark Yukawa y_b [37]. From the phenomenological point of view, it is, therefore, important to explore the possibility that the light-quark Yukawa couplings and/or their interactions with the gauge boson's are significantly enhanced or modified with respect to the SM. Indeed, there has recently been a growing interest in the study of light-quark's Yukawa couplings, see e.g., [38–46]. For example, in [39, 40], the Higgs p_T distributions in inclusive Higgs production, $pp \rightarrow h + X$, was used to study the sensitivity to y_q , where it was shown that the measurements from the 8 TeV LHC run constrain the Yukawa couplings of the 1st generation quarks and the c-quark to be $y_u, y_d \lesssim 0.5y_b$ [39] and $y_c \lesssim 5y_b$ [40], respectively. Slightly improved bounds are expected in the inclusive channel at the future LHC Runs: $y_u, y_d \lesssim 0.3y_b$ [39, 41] and $y_c \lesssim y_b$ [40]. As we will see below, a p_T -dependent ratio between the NP and SM cross-sections (the signal strength) for the exclusive Higgs + jet production cross-section, $\sigma(pp \rightarrow h + j)$, followed by the Higgs decays to e.g., $\gamma\gamma$ and WW^* , may be used to put comparable and, in some cases, stronger constraints on y_q . In particular, we will show that, if the ggh effective coupling also deviates from its SM value, then significantly stronger bounds on y_q are expected.

We also explore exclusive Higgs + jet production in the SMEFT, defined as the expansion of the SM Lagrangian with an infinite series of higher dimensional effective operators. We find that the exclusive $pp \rightarrow h + j(j_b)$ signal can probe the NP scenarios portrayed by the SMEFT with typical scales ranging from a few to $\mathcal{O}(10)$ TeV, depending on the details of underlying physics.

The paper is organized as follows: in section II we outline our notation and define our observables for the study of NP in $pp \rightarrow h + j$ and $pp \rightarrow h + j_b$. In sections III and IV we discuss the NP effects in $pp \rightarrow h + j(j_b)$ within the kappa and the SMEFT frameworks, respectively, and in section V we summarize.

II. NOTATION AND OBSERVABLES

We define the signal strength for $pp \rightarrow h + j$ (and similarly for $pp \rightarrow h + j_b$), followed by the Higgs decay $h \rightarrow ff$, where f can be any of the SM Higgs decay products (e.g., $f = b, \tau, \gamma, W, Z$), as the ratio of the number of $pp \rightarrow h + j \rightarrow ff + j$ events in some NP scenario relative to the corresponding number of Higgs events in the SM:

$$\mu_{hj}^f = \frac{\mathcal{N}(pp \rightarrow h + j \rightarrow ff + j)}{\mathcal{N}_{SM}(pp \rightarrow h + j \rightarrow ff + j)}. \quad (9)$$

In particular, \mathcal{N} is the event yield $\mathcal{N} = \mathcal{L}\sigma\mathcal{A}\epsilon$, where \mathcal{L} is the luminosity, \mathcal{A} is the acceptance in the signal analysis (i.e., the fraction of events that "survive" the

cuts) and ϵ is the efficiency which represents the probability that the fraction of events that pass the set of cuts are correctly identified. Clearly, the luminosity and efficiency factors, \mathcal{L} and ϵ , cancel by definition in μ_{hj}^f of Eq. 9, whereas the acceptance factors, \mathcal{A} and \mathcal{A}_{SM} , do not in general, unless the NP in the numerator of μ_{hj}^f does not change the kinematics of the events. Given the exploratory nature of this work, we will assume, for simplicity, that $\mathcal{A} \simeq \mathcal{A}_{SM}$ in Eq. 9, in which case one obtains:^[1]

$$\mu_{hj}^f \simeq \frac{\sigma(pp \rightarrow h + j)}{\sigma_{SM}(pp \rightarrow h + j)} \cdot \frac{BR(h \rightarrow ff)}{BR_{SM}(h \rightarrow ff)}. \quad (10)$$

We further assume that there is no NP in the Higgs decay $h \rightarrow ff$ and, for definiteness, we will occasionally consider the decay channel $h \rightarrow \gamma\gamma$ (i.e., with a SM rate), at the LHC with a luminosity of $300 fb^{-1}$ and/or $3000 fb^{-1}$ (corresponding to the high-luminosity LHC, HL-LHC), representing the lower and higher statistics cases for the Higgs + jet signal $pp \rightarrow h + j \rightarrow \gamma\gamma + j$.

We will henceforward use the p_T -dependent "cumulative cross-section", satisfying a given lower Higgs p_T cut, as follows:

$$\sigma(p_T^{cut}) \equiv \sigma(p_T(h) > p_T^{cut}) = \int_{p_T(h) \geq p_T^{cut}} dp_T \frac{d\sigma}{dp_T}, \quad (11)$$

which turns out to be useful for minimizing the ratio between the higher-order and LO $pp \rightarrow h + j$ cross-sections (i.e., the K-factor) for values of $p_T^{cut} \gtrsim 150$ GeV [8, 11]. Furthermore, as was mentioned earlier and will be shown below, the p_T -distribution of the Higgs may be sensitive to the specific type of the underlying NP, so that the cumulative cross-section of Eq. 11 gives an extra handle for extracting the NP effects in $pp \rightarrow h + j$, without having to analyze fully differential quantities associated with $pp \rightarrow h + j$.

All cross-sections are calculated using MadGraph5 [47], where a dedicated universal FeynRules output (UFO) model was produced for the MadGraph5 sessions using FeynRules [48], for both the kappa and SMEFT frameworks. The analytical results were cross-checked with Formcalc [49], while intermediate steps were validated using FeynCalc [50]. We use the LO MSTW 2008 PDF set [51], in the 4 flavor and 5 flavor schemes MSTW2008lo68clnf4 and MSTW2008lo68cl, respectively, with a dynamical scale choice for the central value of the factorization (μ_F) and renormalization (μ_R) scales, corresponding to the sum of the transverse mass in the hard-process level: $\mu_F = \mu_R = \mu_T \equiv \sum_i \sqrt{m_i^2 + p_T^2(i)} = \sqrt{m_h^2 + p_T^2(h)} + p_T(j)$. The uncertainty in μ_F and μ_R is evaluated by varying them in

[1] The effect of $\mathcal{A} \neq \mathcal{A}_{SM}$ can be estimated by simulating the detector acceptance in the actual analysis, and scaling our results below (for the signal strength μ_{hj}^f) by the factor $\mathcal{A}/\mathcal{A}_{SM}$.

the range $\frac{1}{2}\mu_T \leq \mu_F, \mu_R \leq 2\mu_T$. As mentioned above, all cross-sections were calculated with a lower $p_T(h)$ cut and, in some instances, an overall invariant mass cut was imposed using Mad-Analysis5 [52]. The rest of the cuts were set to their default values in MadGraph5.

To study the sensitivity of μ_{hj}^f to NP we define our NP signal to be (recall that $\mu_{hj}^f(SM) = 1$):

$$\Delta\mu_{hj}^f \equiv | \mu_{hj}^f - 1 | , \quad (12)$$

and assume that μ_{hj}^f will be measured to a given accuracy $\delta\mu_{hj,exp}^f(1\sigma)$, with a central value $\hat{\mu}_{hj,exp}^f$:

$$\mu_{hj,exp}^f = \hat{\mu}_{hj,exp}^f \pm \delta\mu_{hj,exp}^f(1\sigma) . \quad (13)$$

Thus, taking $\hat{\mu}_{hj,exp}^f = \mu_{hj}^f$ (μ_{hj}^f being our prediction for the measured value $\hat{\mu}_{hj,exp}^f$), the statistical significance of the NP signal is:

$$N_{SD} = \frac{\Delta\mu_{hj}^f}{\delta\mu_{hj}^f} , \quad (14)$$

which we will use in the following analysis, where $\delta\mu_{hj}^f$ represents the combined experimental and theoretical 1σ error, e.g., $\delta\mu_{hj}^f = \sqrt{(\delta\mu_{hj,theory}^f)^2 + (\delta\mu_{hj,exp}^f)^2}$. In particular, in the spirit of the ultimate goal of the Higgs physics program, which is to reach a percent level accuracy in the measurements and calculations of Higgs production and decay modes [53], we will assume throughout this work that the signal strength defined above, for Higgs+jet production followed by the Higgs decay, will be measured and known to a 5%(1 σ) accuracy. That is, that the combined experimental and theoretical uncertainties will be pushed down to $\delta\mu_{hj}^f = 0.05(1\sigma)$. Indeed, achieving such an accuracy is both a theoretical and experimental challenge, which, however, seems to be feasible in the LHC era with the large statistics expected in the future runs and in light of the recent progress made in higher-order calculations.

III. HIGGS + JET PRODUCTION IN THE KAPPA-FRAMEWORK

The kappa-framework is defined by multiplying the SM couplings g_i by a scaling factor κ_i , which parameterizes the effects of NP when it has the same Lorentz structure as the corresponding SM interactions [54, 55]. In the case of $pp \rightarrow h + j(j_b)$, the relevant scaling factors apply to the effective (1-loop) Higgs-gluon interaction of Eq. 4 and to the light and/or b-quark Yukawa couplings. In particular, the effective interaction Lagrangian for $pp \rightarrow h + j(j_b)$ in the kappa-framework, takes the form:

$$\mathcal{L}_{eff}^{h+j} = - \sum_{q=u,d,s,c,b} \kappa_q \frac{m_b}{v} h\bar{q}q + \kappa_g C_g h G_{\mu\nu}^a G^{\mu\nu,a} , \quad (15)$$

where we have scaled the light-quark Yukawa coupling, y_q , with the SM b-quark Yukawa:

$$\kappa_q \equiv \frac{y_q}{y_b^{SM}} , \quad (16)$$

and $y_b^{SM} = \sqrt{2}m_b/v$. In particular, $\kappa_g = 1$, $\kappa_b = 1$, $\kappa_c \sim 0.3$, $\kappa_s \sim \mathcal{O}(10^{-2})$ and $\kappa_{u,d} \sim \mathcal{O}(10^{-3})$ are the SM strengths for the corresponding couplings. In what follows, we will refer to the SM case by $\kappa_{u,d,c,s} = 0$, since the effect of the small SM values for $\kappa_{u,d,c,s}$ in $pp \rightarrow h + j$ are negligible.

A. The case of Higgs + light-jet production

As mentioned earlier, in the case of $pp \rightarrow h + j$, where $j = g, u, d, s, c$ is a non-flavor tagged light-jet originating from a gluon or any quark of the 1st and 2nd generations, the SM tree-level diagrams involving the light-quarks Yukawa couplings are vanishingly small (see Eqs. 1-3). Therefore, the dominant SM contribution to $\sigma(pp \rightarrow h + j)$ arises at 1-loop via the sub-processes $gg \rightarrow gh$, $gq \rightarrow qh$, $g\bar{q} \rightarrow \bar{q}h$ and $q\bar{q} \rightarrow gh$ (the corresponding diagrams are depicted in Fig. 2, where the loops are represented by an effective ggh vertex). In particular, using the Higgs-gluon effective Lagrangian of Eq. 4, the corresponding total SM cross-section for $pp \rightarrow h + j$ can be written as:

$$\sigma_{SM}^{hj} = C_g^2 (\sigma_{SM}^{gg} + \sigma_{SM}^{gq} + \sigma_{SM}^{g\bar{q}} + \sigma_{SM}^{q\bar{q}}) , \quad (17)$$

where σ_{SM}^{ij} , for $ij = gg, gq, g\bar{q}, q\bar{q}$, can be obtained from the corresponding squared amplitudes given in Eqs. 5-8. For example, σ_{SM}^{gg} is to the part of the SM cross-section coming from $gg \rightarrow gh$, which is the dominant sub-process in the SM.

On the other hand, turning on the light-quark qqh Yukawa couplings and allowing for deviations also in the Higgs-gluon ggh interaction, within the kappa-framework of Eq. 15, we obtain the total NP cross-section for $pp \rightarrow h + j$:

$$\sigma^{hj} = \kappa_g^2 \sigma_{SM}^{hj} + \kappa_q^2 \sigma_{qqh}^{hj} , \quad (18)$$

where $\sigma_{SM}^{hj} \simeq \sigma^{hj}(\kappa_g = 1, \kappa_q = 0)$ is given in Eq. 17 and $\sigma_{qqh}^{hj} = \sigma^{hj}(\kappa_g = 0, \kappa_q = 1)$ arises from the the s-channel and t-channel tree-level $gq \rightarrow qh$ diagrams, depicted in Fig. 1, where only the (scaled) light-quarks qqh Yukawa couplings contribute. The interference term between the diagrams involving the ggh and qqh couplings is proportional to the light-quark mass and is, therefore, neglected in Eq. 18. In particular, σ^{hj} is practically insensitive to the signs of κ_g and κ_q .

Furthermore, in the $hgg - h\bar{q}q$ kappa-framework of Eq. 15, the ratio of branching ratios in Eq. 10 is given

by:

$$\begin{aligned} \mu_{h \rightarrow ff} &\equiv \frac{BR(h \rightarrow ff)}{BR_{SM}(h \rightarrow ff)} \\ &= \frac{1}{1 + (\kappa_g^2 - 1) BR_{SM}^{gg} + \kappa_q^2 BR_{SM}^{bb}}, \end{aligned} \quad (19)$$

where $BR_{SM}^{gg,bb} = BR_{SM}(h \rightarrow gg, bb)$ and we will assume no NP in the Higgs decay $h \rightarrow ff$. In particular, as mentioned above, we assume that the Higgs decays via $h \rightarrow \gamma\gamma$ with a SM decay rate.

Collecting the expressions from Eqs. 10, 18 and 19, we obtain the signal strength in the kappa-framework:

$$\mu_{hj}^f = (\kappa_g^2 + \kappa_q^2 R^{hj}) \cdot \mu_{h \rightarrow ff}, \quad (20)$$

where

$$R^{hj} \equiv \frac{\sigma_{qqh}^{hj}}{\sigma_{SM}^{hj}}, \quad (21)$$

is the NP contribution scaled with the SM cross-section and calculated using cumulative cross-sections, as defined in Eq. 11, i.e., for a given p_T^{cut} in both numerator and denominator: $R^{hj} = R^{hj}(p_T^{cut}) = \sigma_{qqh}^{hj}(p_T^{cut})/\sigma_{SM}^{hj}(p_T^{cut})$. The ratio R^{hj} contains all the dependence of μ_{hj}^f on the Higgs p_T and, as will be further discussed below, is where all the uncertainties reside, i.e., the higher order corrections (K-factor), the normalization and factorization scale uncertainties of the PDF and the acceptance factors.

In Fig. 3 we show the dependence of R^{hj} and the signal strength, μ_{hj}^f , on p_T^{cut} , assuming no NP in the hgg interaction ($\kappa_g = 1$) and for the cases in which either a single or all light-quark Yukawa couplings are modified, i.e., $\kappa_q = 1$ for any one of the light-quarks $q = u, d, s, c$ or $\kappa_q = 1$ for all $q = u, d, s, c$. We find that the effect of $\kappa_q \neq 0$ is to change the softer $p_T(h)$ spectrum, so that R^{hj} drops when p_T^{cut} is increased. As a result, the contribution of κ_q to $pp \rightarrow h + j$ sharply drops in the harder $p_T(h)$ region, $p_T(h) \gtrsim 300$ GeV, where $R^{hj} \lesssim \mathcal{O}(0.1)$, see Fig. 3.

Note, however, that the signal strength approaches an asymptotic value as p_T^{cut} is further increased, which corresponds to the region where the κ_q dependence of μ_{hj}^f is dominated by the decay factor $\mu_{h \rightarrow ff}$ in Eq. 19. In particular, $\mu_{hj}^f \rightarrow 0.6 - 0.7$ in the single $\kappa_q = 1$ case and $\mu_{hj}^f \rightarrow 0.3$ when $\kappa_q = 1$ for all light-quarks. Thus, in the high Higgs p_T regime, the difference between the effects of a single $\kappa_q \neq 0$ is small, i.e., for either of the quark flavors $q = u, d, c, s$. The advantage of monitoring the high $p_T(h)$ spectrum, where R^{hj} is suppressed is, therefore, reducing the theoretical and experimental uncertainties which, as mentioned above, reside only in R^{hj} . Indeed, this will be illustrated in Table I below, where we show the sensitivity of the signal to the PDF scale uncertainty.

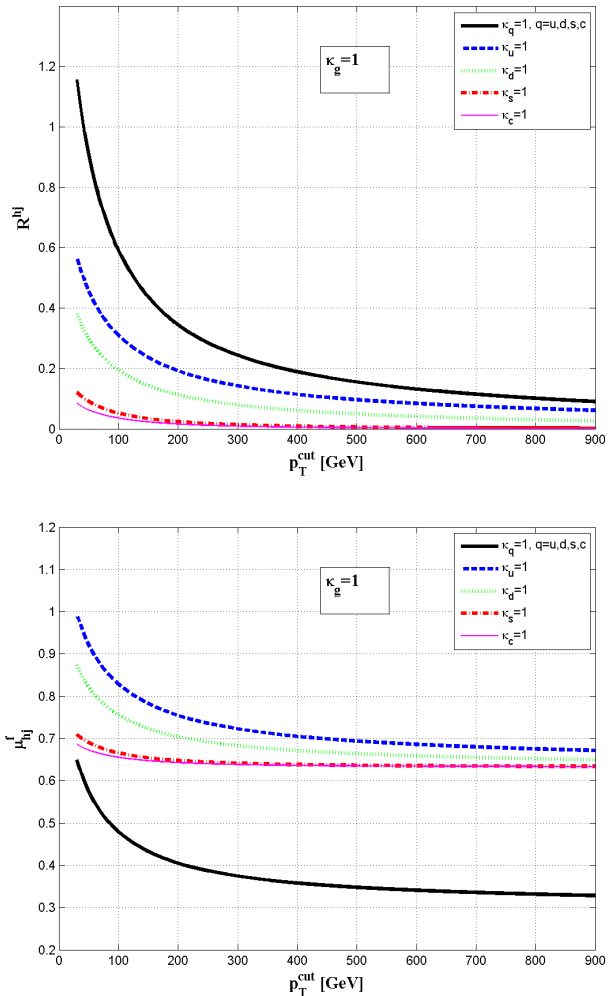


FIG. 3: The p_T^{cut} dependence of R^{hj} (top) and μ_{hj}^f (bottom), for $\kappa_g = 1$ (i.e., assuming no NP in the hgg interaction) and the cases $\kappa_q = 1$ for all $q = u, d, s, c$ (solid line), $\kappa_u = 1$ (dashed line), $\kappa_d = 1$ (dotted line), $\kappa_s = 1$ (dot-dashed line) and $\kappa_c = 1$ (thin solid line).

In Fig. 4 we plot the expected statistical significance, N_{SD} defined in Eq. 14, assuming a 5% relative error ($\delta\mu_{hj}^f = 0.05$), as a function of κ_q for two cases: (i) $\kappa_q \neq 0$ for all $q = u, d, s, c$ and (ii) only $\kappa_u \neq 0$. In both cases we assume no NP in the Higgs-gluon coupling ($\kappa_g = 1$) and we use two different p_T^{cut} values $p_T^{cut} = 100, 400$ GeV. We see that, in the single $\kappa_u \neq 0$ case, there is a 3σ sensitivity to values of $\kappa_u \gtrsim 0.6$, for $\kappa_g = 1$ and using $p_T^{cut} = 400$ GeV. In the case where the NP modifies κ_q for all $q = u, d, c, s$, one can expect a deviation of more than 3σ for values of $\kappa_q \gtrsim 0.3$. We also show in Fig. 4 the corresponding expected number of $pp \rightarrow h + j \rightarrow \gamma\gamma + j$ events, as a function of κ_q for cases (i) and (ii) considered above, with $p_T^{cut} = 100$ and 400 GeV and an integrated luminosity of 300 and 3000 fb^{-1} , respectively,

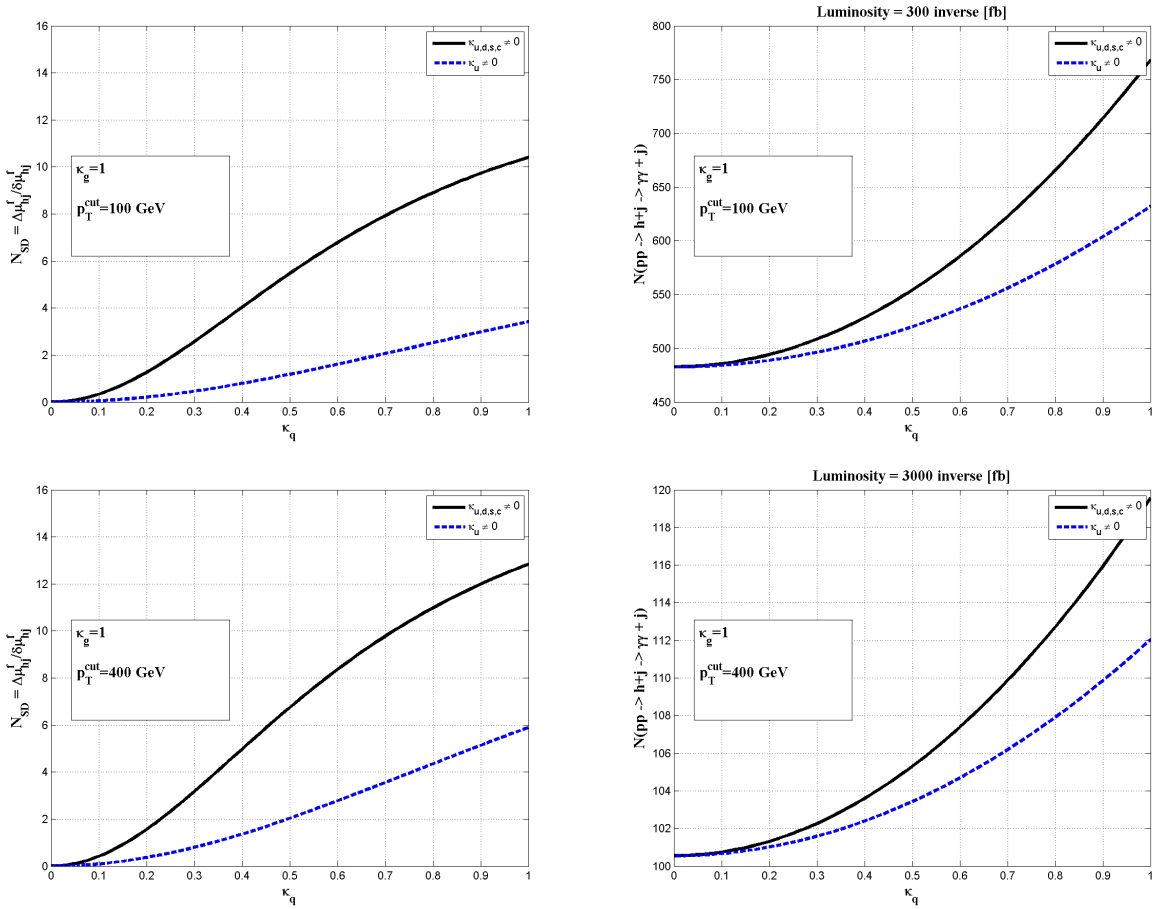


FIG. 4: The expected statistical significance, $N_{SD} = \Delta\mu_{hj}^f/\delta\mu_{hj}^f$, and the number of $pp \rightarrow h + j \rightarrow \gamma\gamma + j$ events, as a function of κ_q , for $\kappa_g = 1$ (i.e., assuming no NP in the hgg interaction) and for $p_T^{cut} = 100$ GeV (upper plots) and $p_T^{cut} = 400$ GeV (lower plots). The two cases of a single $\kappa_u \neq 0$ (dashed line) and $\kappa_q \neq 0$ for all $q = u, d, s, c$ (solid line), are considered. We assume a 5% relative error ($\delta\mu_{hj}^f = 0.05$) and an acceptance of 50% in the event yield, with a luminosity of $\mathcal{L} = 300 \text{ fb}^{-1}$ for the $p_T^{cut} = 100$ GeV case and $\mathcal{L} = 3000 \text{ fb}^{-1}$ in the $p_T^{cut} = 400$ GeV case.

assuming a signal acceptance of 50%. We can see that around 1000(100) $pp \rightarrow h + j \rightarrow \gamma\gamma + j$ events with $p_T(h) > 100(400)$ GeV are expected at the LHC(HL-LHC), i.e., with $\mathcal{L} = 300(3000) \text{ fb}^{-1}$. Thus, in both cases it should be possible to probe the NP effects when the Higgs decays via $h \rightarrow \gamma\gamma$.

The signal strength μ_{hj}^f is more sensitive to NP in the Higgs-gluon coupling, i.e., to κ_g . We find, for example, that if μ_{hj}^f is known to a 5%(1 σ) accuracy, then a deviation of more than 3σ is expected for $\kappa_q \lesssim 0.9$ for any value of κ_q and for any $p_T^{cut} \lesssim 500$ GeV. This is illustrated in Fig. 5 where we plot the 68%, 95% and 99% confidence level (CL) allowed ranges in the $\kappa_q - \kappa_g$ plane, for $p_T^{cut} = 400$ GeV and assuming that the signal strength has been measured to be $\mu_{hj}^f \sim 1 \pm 0.05(1\sigma)$, i.e., with a SM central value and to an accuracy of $\delta\mu_{hj}^f = 5\%(1\sigma)$. Here also, we consider both the single κ_u case where $\kappa_u \neq 0$ and $\kappa_d = \kappa_s = \kappa_c = 0$ and the case where $\kappa_q \neq 0$

for all $q = u, d, s, c$. In particular, values of $\{\kappa_q, \kappa_g\}$ outside the shaded 99% contour will be excluded at more than 3σ , if the signal strength will be measured to lie within $0.85 < \mu_{hj}^f < 1.15$.

In Table I we list the statistical significance of the NP signal, $N_{SD} = \Delta\mu_{hb}^f/\delta\mu_{hb}^f$, as defined in Eq. 14, again assuming 5% error ($\delta\mu_{hj}^f = 0.05(1\sigma)$), for $p_T^{cut} = 400$ GeV and some discrete values of the scaled couplings: $\kappa_q = 0, 0.25, 0.5$ and $\kappa_g = 0.8, 0.9, 1, 1.1, 1.2$. Here also, results are given in the single κ_u case and in the case where $\kappa_q \neq 0$ for all $q = u, d, s, c$. We include the PDF scale dependence and (although of little use) write N_{SD} up to the 2nd digit to illustrate the small uncertainty due the PDF scale. Note that for $\kappa_q = 0$ there is no dependence on the PDF scale since, in this case, it is cancelled in the ratio of cross-sections as defined in the signal strength μ_{hj}^f . We see that indeed the effect of the PDF scale dependence is negligible due to the smallness of R^{hj} in the harder p_T spectrum, in particular for $p_T^{cut} =$

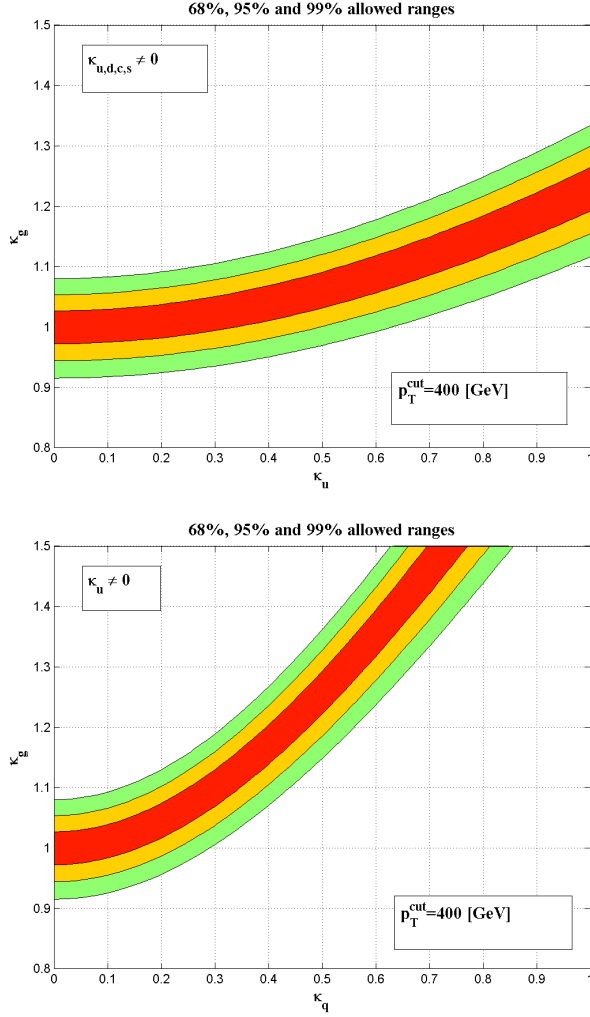


FIG. 5: The 68%(red), 95%(orange) and 99%(green) CL sensitivity ranges, corresponding to $\Delta\mu_{hj}^f \equiv |\mu_{hj}^f - 1| \leq 0.05, 0.1$ and 0.15 , respectively, with $p_T^{cut} = 400$ GeV, in the $\kappa_u - \kappa_g$ plane for $\kappa_d = \kappa_s = \kappa_c = 0$ (top) and in the $\kappa_q - \kappa_g$ plane for $\kappa_q = \kappa_u = \kappa_d = \kappa_s = \kappa_c$ (bottom). Recall that $\kappa_g = 1$ and $\kappa_{u,d,c,s} \rightarrow 0$ represent the SM case, see also text.

400 GeV used in the Table I (see also discussion above).

B. The case of Higgs + b-jet production

We next turn to Higgs + b-jet production, which can be described in the five flavor scheme (5FS), where one treats the b-quark as a massless parton while keeping its Yukawa coupling finite [56], see also [57, 58]. In particular, the LO contribution to $pp \rightarrow h + j_b$ arises at tree-level by the same diagrams that drive the subprocess $qg \rightarrow hq$ (and the charged conjugate one $g\bar{b} \rightarrow \bar{b}h$), shown in Fig. 1 with $q = b$. The cross-section for these diagrams is pro-

$$\text{Statistical significance } N_{SD} = \frac{\Delta\mu_{hj}^f}{\delta\mu_{hj}^f}$$

$$\kappa_u \neq 0, \kappa_d = \kappa_s = \kappa_c = 0$$

	$\kappa_u = 0$	$\kappa_u = 0.25$	$\kappa_u = 0.5$
$\kappa_g = 0.8$	6.79	$7.12_{+0.03}^{-0.03}$	$8.0_{+0.10}^{-0.11}$
$\kappa_g = 0.9$	3.53	$3.97_{+0.03}^{-0.03}$	$5.14_{+0.10}^{-0.11}$
$\kappa_g = 1.0$	0	$0.56_{+0.03}^{-0.03}$	$2.03_{+0.10}^{-0.11}$
$\kappa_g = 1.1$	3.78	$3.09_{+0.03}^{-0.03}$	$1.30_{+0.10}^{-0.11}$
$\kappa_g = 1.2$	7.75	$6.95_{+0.03}^{-0.03}$	$4.84_{+0.10}^{-0.11}$

$$\kappa_q \neq 0 \text{ for all } q = u, d, s, c$$

	$\kappa_q = 0$	$\kappa_q = 0.25$	$\kappa_q = 0.5$
$\kappa_g = 0.8$	6.79	$8.30_{+0.04}^{-0.05}$	$11.13_{+0.12}^{-0.13}$
$\kappa_g = 0.9$	3.53	$5.43_{+0.04}^{-0.05}$	$9.03_{+0.12}^{-0.13}$
$\kappa_g = 1.0$	0	$2.32_{+0.04}^{-0.05}$	$6.74_{+0.12}^{-0.13}$
$\kappa_g = 1.1$	3.78	$1.01_{+0.04}^{-0.05}$	$4.26_{+0.12}^{-0.13}$
$\kappa_g = 1.2$	7.75	$4.55_{+0.04}^{-0.04}$	$1.61_{+0.11}^{-0.13}$

TABLE I: The statistical significance of the NP signal for $pp \rightarrow h + j$, $N_{SD} = \Delta\mu_{hj}^f/\delta\mu_{hj}^f$, assuming a 5% error ($\delta\mu_{hj}^f = 0.05(1\sigma)$), for $p_T^{cut} = 400$ GeV and for values of the scaled couplings $\kappa_q = 0, 0.25, 0.5$ and $\kappa_g = 0.8, 0.9, 1, 1.1, 1.2$, in the single κ_u case assuming $\kappa_d = \kappa_s = \kappa_c = 0$ (top table) and in the case where $\kappa_q \neq 0$ for all $q = u, d, s, c$ (bottom table). The errors indicate the PDF scale dependence, where the superscript(subscript) corresponds to twice(half) the nominal scale $\mu_F = \mu_R = \mu_T \equiv \sum_i \sqrt{m_i^2 + p_T^2(i)}$, see also text.

portional to the bbh Yukawa coupling (squared) and can be obtained from the corresponding squared amplitudes which are given in Eqs. 1-3. The 1-loop contribution to $gb \rightarrow bh$, which, in the infinite top-quark mass limit, can be described by the effective ggh vertex (see Fig. 2), is given in Eqs. 6-8. It is comparable to the LO tree-level one at low $p_T(h) \lesssim 100$ GeV, while it dominates at the higher $p_T(h)$ spectrum (see below).^[2]

Let us denote the corresponding tree-level and 1-loop cumulative cross-sections (following Eq. 11) for $pp \rightarrow h + j_b$ as $\sigma_{bbh}^{hj_b} \equiv \sigma_{bbh}^{hj_b}(p_T^{cut})$ and $\sigma_{ggh}^{hj_b} \equiv \sigma_{ggh}^{hj_b}(p_T^{cut})$, respectively. Thus, in the kappa-framework where κ_b and κ_g are the only NP scaled couplings, the total Higgs + b-jet cross-section is (again there is negligible interference between the diagrams involving the bbh and ggh interactions):

$$\sigma^{hj_b} = \kappa_g^2 \sigma_{ggh}^{hj_b} + \kappa_b^2 \sigma_{bbh}^{hj_b}, \quad (22)$$

[2] Note that the Higgs + light-jet processes (in particular, the dominant gluon-fusion process $gg \rightarrow hg$) may "contaminate" the Higgs + b-jet signal, when the light jet is mistagged as a b-jet. The probability for that is, however, expected to be at the sub-percent level for a b-tagging efficiency of $\epsilon_b \sim 60 - 70\%$ and is, therefore, neglected.

so that the SM cross-section is obtained for $\kappa_g = \kappa_b = 1$, i.e., $\sigma_{SM}^{hjb} = \sigma_{ggh}^{hjb} + \sigma_{bbh}^{hjb}$.

The signal strength for $pp \rightarrow h + j_b \rightarrow ff + j_b$ is then given by:

$$\begin{aligned} \mu_{hjb}^f &= \frac{\mathcal{N}(pp \rightarrow h + j_b \rightarrow ff + j_b)}{\mathcal{N}_{SM}(pp \rightarrow h + j_b \rightarrow ff + j_b)} \\ &\simeq \left(\frac{\kappa_g^2}{1 + R^{hjb}} + \frac{\kappa_b^2}{1 + (R^{hjb})^{-1}} \right) \cdot \mu_{h \rightarrow gg}^b, \end{aligned} \quad (23)$$

where

$$R^{hjb} \equiv \frac{\sigma_{bbh}^{hjb}}{\sigma_{ggh}^{hjb}}, \quad (24)$$

and

$$\begin{aligned} \mu_{h \rightarrow ff}^b &\equiv \frac{BR(h \rightarrow ff)}{BR_{SM}(h \rightarrow ff)} \\ &= \frac{1}{1 + (\kappa_g^2 - 1) BR_{SM}^{gg} + (\kappa_b^2 - 1) BR_{SM}^{bb}} \end{aligned} \quad (25)$$

Once again, all the uncertainties associated with the measurement of μ_{hjb}^f reside in the ratio of cross-sections R^{hjb} and in the limit $R^{hjb} \ll 1$, we get an expression for μ_{hjb}^f which is similar to the one obtained for the Higgs + light-jet case in Eq. 20, with the replacement $\kappa_g \rightarrow \kappa_b$:

$$\mu_{hjb}^f (R^{hjb} \ll 1) \simeq (\kappa_g^2 + \kappa_b^2 R^{hjb}) \cdot \mu_{h \rightarrow ff}^b. \quad (26)$$

In particular, we find that, as in the Higgs + light-jet case, the κ_b term is important for softer $p_T(h)$ for which $R^{hjb} \sim \mathcal{O}(1)$, while the κ_g contribution is dominant at the harder $p_T(h)$ regime, where $R^{hjb} \ll 1$. For example, we obtain $R^{hjb} \sim 2$ for $p_T^{cut} \sim 35$ GeV, dropping to $R^{hjb} \sim 1$ at $p_T^{cut} \sim 90$ GeV (i.e., the point where σ_{bbh}^{hjb} is comparable to σ_{ggh}^{hjb}), then to $R^{hjb} \sim 0.4$ for $p_T^{cut} \sim 200$ GeV and further to $R^{hjb} \sim 0.15$ at $p_T^{cut} \sim 400$ GeV. Thus, here also, the effects of higher-order corrections and the PDF scale dependence, as well as the acceptance factors, become insignificant when the signal strength is evaluated for a high $p_T^{cut} \sim 400$ GeV, for which $R^{hjb} \sim \mathcal{O}(0.1)$.

In Fig. 6 we show the dependence of the signal strength μ_{hjb}^f on p_T^{cut} , assuming no NP in the Higgs-gluon ggh interaction ($\kappa_g = 1$) and for values of κ_b within $0 < \kappa_b < 1.5$, which are consistent with the current measurements of the 125 GeV Higgs production and decay processes [59]. We see that, once again, the signal strength approaches an asymptotic value (for a given κ_b value) as p_T^{cut} is increased, which is where the κ_g term dominates and the κ_b dependence arises mostly from the decay factor $\mu_{h \rightarrow ff}^b$ in Eq. 25.

We also show in Fig. 6 the expected number of $pp \rightarrow h + j_b \rightarrow \gamma\gamma + j_b$ events, $N(pp \rightarrow h + j_b \rightarrow \gamma\gamma + j_b) = \mathcal{L} \cdot \sigma(pp \rightarrow h + j_b) \cdot BR(h \rightarrow \gamma\gamma) \cdot \mathcal{A} \cdot \epsilon_b$, as a function of p_T^{cut} at the HL-LHC with $\mathcal{L} = 3000 \text{ fb}^{-1}$, an acceptance

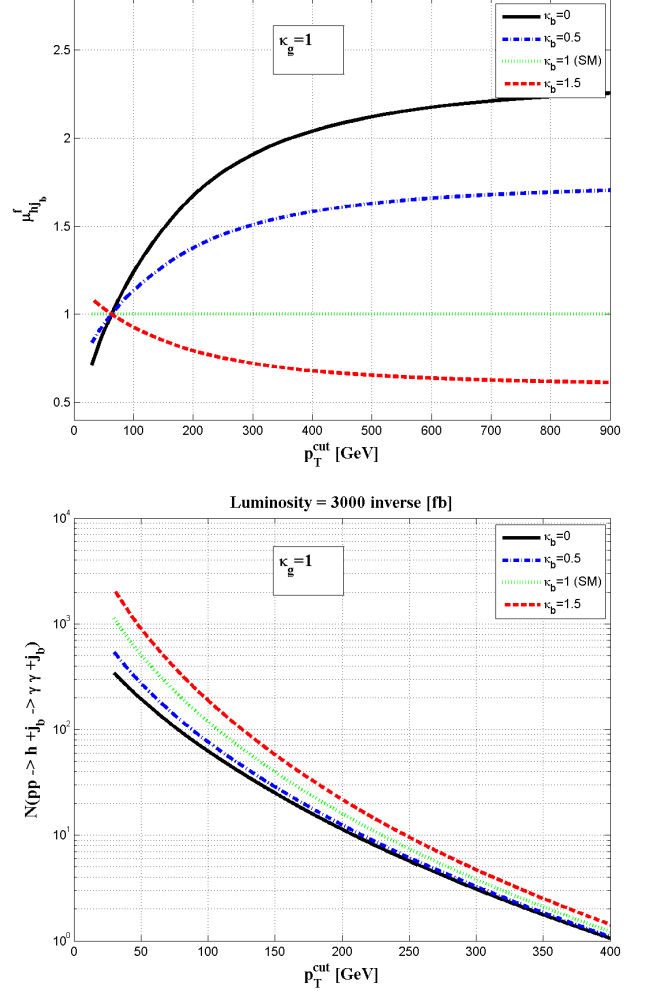


FIG. 6: The p_T^{cut} dependence of μ_{hjb}^f (top) and of the expected number of events $N(pp \rightarrow h + j_b \rightarrow \gamma\gamma + j_b) = \mathcal{L} \cdot \sigma(pp \rightarrow h + j_b) \cdot BR(h \rightarrow \gamma\gamma) \cdot \mathcal{A} \cdot \epsilon_b$ (bottom) at the HL-LHC with $\mathcal{L} = 3000 \text{ fb}^{-1}$, an acceptance of $\mathcal{A} = 0.5$ and a b-jet tagging efficiency of $\epsilon_b = 0.7$. The curves are for $\kappa_g = 1$ (i.e., assuming no NP in the ggh interaction) and for $\kappa_b = 0, 0.5, 1, 1.5$ ($\kappa_b = 1$ corresponds to the SM case where $\mu_{hjb}^f = 1$).

of $\mathcal{A} = 0.5$ and a b-jet tagging efficiency of 70%, i.e., $\epsilon_b = 0.7$. We see that, under these conditions and for the values of κ_g and κ_b considered, a $p_T^{cut} \lesssim 100$ GeV is required to ensure $\mathcal{O}(100)$ $pp \rightarrow h + j_b \rightarrow \gamma\gamma + j_b$ events. In particular, $\mathcal{N}(pp \rightarrow h + j_b \rightarrow \gamma\gamma + j_b) \sim \mathcal{O}(1000)$ for $p_T^{cut} \sim 30$ GeV and $\mathcal{N}(pp \rightarrow h + j_b \rightarrow \gamma\gamma + j_b) \sim \mathcal{O}(10)$ for $p_T^{cut} \sim 200$ GeV, respectively.

In the following, we will therefore use $p_T^{cut} = 30$ GeV and 200 GeV as two representative extreme cases, where the former can be detected in the $pp \rightarrow h + j_b \rightarrow \gamma\gamma + j_b$ channel, while the latter is more suited for a higher statistics channel, such as $pp \rightarrow h + j_b \rightarrow WW^* + j_b$ followed by the leptonic W-decays $WW^* \rightarrow 2\ell 2\nu$, which

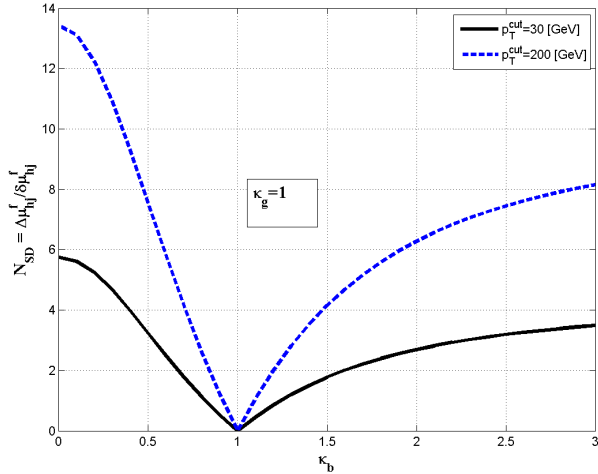


FIG. 7: The statistical significance, $N_{SD} = \Delta\mu_{hjb}^f / \delta\mu_{hjb}^f$, as a function of κ_b for $p_T^{cut} = 30$ GeV (solid line) and $p_T^{cut} = 200$ GeV (dashed line), assuming $\kappa_g = 1$ and a 5%(1 σ) error $\delta\mu_{hjb}^f = 0.05$. See also text.

Statistical significance $N_{SD} = \frac{\Delta\mu_{hjb}^f}{\delta\mu_{hjb}^f}$					
	$\kappa_b = 0.5$	$\kappa_b = 0.75$	$\kappa_b = 1$	$\kappa_b = 1.25$	$\kappa_b = 1.5$
$\kappa_g = 0.8$	$0.4_{-0.3}^{+0.6}$	$2.8_{-0.08}^{+0.08}$	$4.6_{+0.3}^{-0.3}$	$6.0_{+0.6}^{-0.6}$	$6.9_{+0.7}^{-0.7}$
$\kappa_g = 0.9$	$3.5_{+0.8}^{-0.8}$	$0.2_{+0.3}^{-0.08}$	$2.4_{+0.2}^{-0.2}$	$4.3_{+0.4}^{-0.4}$	$5.6_{+0.7}^{-0.7}$
$\kappa_g = 1.0$	$7.5_{+1.0}^{-1.0}$	$3.3_{+0.5}^{-0.4}$	0	$2.4_{+0.3}^{-0.3}$	$4.2_{+0.6}^{-0.6}$
$\kappa_g = 1.1$	$11.8_{+1.3}^{-1.3}$	$6.7_{+0.7}^{-0.7}$	$2.6_{+0.2}^{-0.2}$	$0.4_{+0.2}^{-0.2}$	$2.6_{+0.5}^{-0.5}$
$\kappa_g = 1.2$	$16.1_{+1.5}^{-1.5}$	$10.2_{+0.9}^{-0.9}$	$5.3_{+0.3}^{-0.3}$	$1.7_{+0.07}^{-0.07}$	$0.9_{+0.4}^{-0.4}$

TABLE II: The statistical significance of the NP signal for $pp \rightarrow h + j_b$, $N_{SD} = \Delta\mu_{hjb}^f / \delta\mu_{hjb}^f$, assuming $\delta\mu_{hjb}^f = 0.05(1\sigma)$, for $p_T^{cut} = 200$ GeV and for values of the scaled couplings $\kappa_b = 0.5, 0.75, 1, 1.25, 1.5$ and $\kappa_g = 0.8, 0.9, 1, 1.1, 1.2$. The errors indicate the PDF scale dependence, where the superscript(subscript) corresponds to twice(half) the nominal scale $\mu_F = \mu_R = \mu_T \equiv \sum_i \sqrt{m_i^2 + p_T^2(i)}$, see also text.

has a rate about five times larger than $pp \rightarrow h + j_b \rightarrow \gamma\gamma + j_b$. In Fig. 7 we plot the statistical significance of the signals, $N_{SD} = \Delta\mu_{hjb}^f / \delta\mu_{hjb}^f$, for $p_T^{cut} = 30$ and 200 GeV, as a function of κ_b , assuming $\kappa_g = 1$ and a 5%(1 σ) error $\delta\mu_{hjb}^f = 0.05$. We see that, for $p_T^{cut} = 200$ GeV a 3 σ effect is expected if $\kappa_b \lesssim 0.8$ and/or $\kappa_b \gtrsim 1.3$, while for $p_T^{cut} = 30$ GeV a larger deviation from the SM is required, i.e., $\kappa_b \lesssim 0.5$ and/or $\kappa_b \gtrsim 2.2$, for a statistically significant signal of NP in $pp \rightarrow h + j_b \rightarrow \gamma\gamma + j_b$.

In Fig. 8 we plot the 68%, 95% and 99% CL sensitivity ranges of NP in the $\kappa_b - \kappa_g$ plane, for $pp \rightarrow h + j_b$ with $p_T^{cut} = 30$ GeV and $p_T^{cut} = 200$ GeV, assuming again that $\mu_{hj}^f \sim 1 \pm 0.05(1\sigma)$, i.e., around the SM value with a

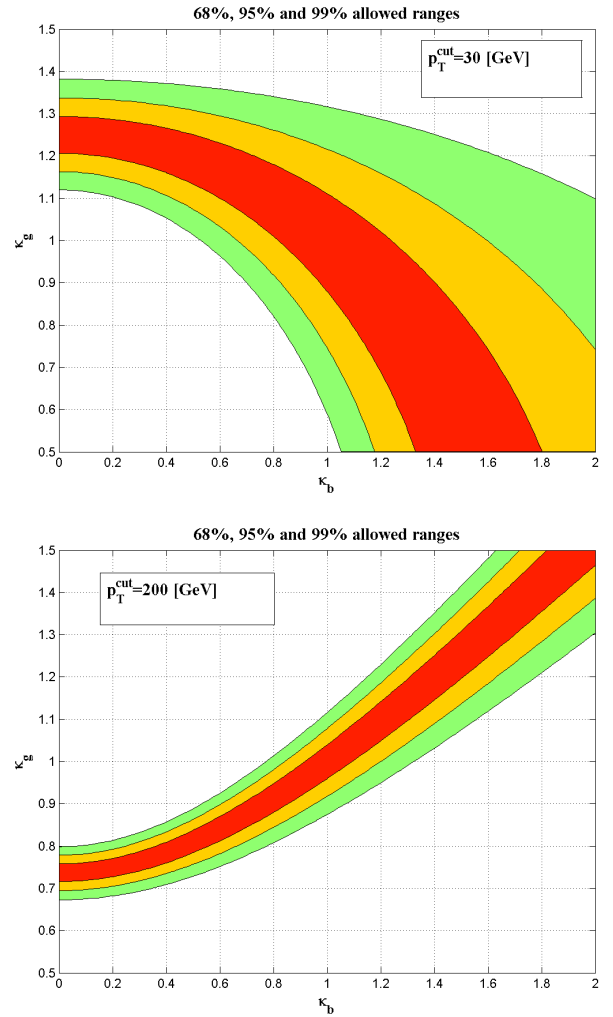


FIG. 8: The 68%(red), 95%(orange) and 99%(green) CL allowed ranges in the $\kappa_b - \kappa_g$ plane, corresponding to $|\mu_{hj}^f - 1| \leq 0.05, 0.1$ and 0.15 , respectively, for $pp \rightarrow h + j_b$ events with $p_T(h) > 30$ GeV (top) and $p_T(h) > 200$ GeV (bottom).

5%(1 σ) accuracy. We see that the two p_T^{cut} cases probe different regimes in the $\kappa_g - \kappa_b$ plane and are, therefore, complementary.

Finally, in Table II we list the statistical significance of NP in $pp \rightarrow h + j_b$, for $\delta\mu_{hjb}^f = 0.05(1\sigma)$, $p_T^{cut} = 200$ GeV and for several discrete values of the scaled couplings: $\kappa_b = 0.5, 0.75, 1, 1.25, 1.5$ and $\kappa_g = 0.8, 0.9, 1, 1.1, 1.2$. Here also we include the PDF scale dependence, which we find to be somewhat higher than in the case of $pp \rightarrow h + j$.

IV. HIGGS + JET PRODUCTION IN THE SMEFT

The SMEFT is defined by expanding the SM Lagrangian with an infinite series of higher dimensional operators, $\mathcal{O}_i^{(n)}$ (using only the SM fields), as [60, 61]:

$$\mathcal{L}_{SMEFT} = \mathcal{L}_{SM} + \sum_{n=5}^{\infty} \frac{1}{\Lambda^{(n-4)}} \sum_i f_i^{(n)} \mathcal{O}_i^{(n)}, \quad (27)$$

where Λ is the scale of the NP that underlies the SM, n denotes the dimension and i all other distinguishing labels.

Considering the expansion up to operators of dimension 6 (for a complete list of dimension 6 operators in the SMEFT, see e.g. [61]), we will study here the following subset of operators that can potentially modify the Higgs + jet production processes:

$$\mathcal{O}_{u\phi} = (\phi^\dagger \phi) (\bar{Q}_L \tilde{\phi} u_R) + h.c., \quad (28)$$

$$\mathcal{O}_{d\phi} = (\phi^\dagger \phi) (\bar{Q}_L \phi d_R) + h.c., \quad (29)$$

$$\mathcal{O}_{ug} = (\bar{Q}_L \sigma^{\mu\nu} T^a u_R) \tilde{\phi} G_{\mu\nu}^a + h.c., \quad (30)$$

$$\mathcal{O}_{dg} = (\bar{Q}_L \sigma^{\mu\nu} T^a d_R) \phi G_{\mu\nu}^a + h.c., \quad (31)$$

$$\mathcal{O}_{\phi g} = (\phi^\dagger \phi) G_{\mu\nu}^a G^{a,\mu\nu}, \quad (32)$$

where ϕ is the SM Higgs doublet (with $\tilde{\phi} \equiv i\sigma_2 \phi^*$), $G^{a,\mu\nu}$ denotes the QCD gauge-field strength and Q_L and $u_R(d_R)$ are the $SU(2)_L$ quark doublet and charge 2/3(-1/3) singlets, respectively.

In particular, we assume that the physics which underlies Higgs+jet production is contained within (dropping the dimension index $n = 6$):

$$\mathcal{L}_{SMEFT} = \mathcal{L}_{SM} + \sum_{i=u\phi, d\phi, ug, dg, \phi g} \frac{f_i}{\Lambda_i^2} \mathcal{O}_i, \quad (33)$$

and, to be as general as possible, we allow different scales of the NP which underly the different operators. For example, $\Lambda_{u\phi}$ corresponds to the typical scale of $\mathcal{O}_{u\phi}$, where by ‘‘typical scale’’ we mean that the corresponding Wilson coefficients is $f_{u\phi} \sim \mathcal{O}(1)$.

The effects of the operators $\mathcal{O}_{u\phi}$, $\mathcal{O}_{d\phi}$ and $\mathcal{O}_{\phi g}$ can be ‘‘mapped’’ into the kappa-framework, satisfying:

$$\kappa_q \simeq \frac{y_q^{SM}}{y_b^{SM}} - \frac{f_{q\phi}}{y_b^{SM}} \frac{v^2}{\Lambda_{q\phi}^2}, \quad \kappa_g = 1 + \frac{12\pi f_{\phi g}}{\alpha_s} \frac{v^2}{\Lambda_{\phi g}^2}, \quad (34)$$

where $y_q^{SM}/y_b^{SM} \rightarrow 0$ for e.g., $q = u$ or d , while $y_q^{SM}/y_b^{SM} = 1$ for the b-quark. Thus, the sensitivity of the signal strength $\mu_{h_j}^f$ for $pp \rightarrow h + j$ (defined in Eqs. 9 and 10) to the effective Lagrangian containing the operators $\mathcal{O}_{u\phi}$, $\mathcal{O}_{d\phi}$ and $\mathcal{O}_{\phi g}$ can be obtained from the analysis that has been performed for the kappa-framework in the previous section. For example, it follows from Eq. 34 that, for $f_{u\phi}$, $f_{\phi g} \sim \mathcal{O}(1)$, one expects $|\kappa_u| \lesssim 0.5$ and

$\Delta\kappa_g = |\kappa_g - 1| \gtrsim 0.1$, if the corresponding scales of NP are $\Lambda_{u\phi} \gtrsim 3$ TeV and $\Lambda_{\phi g} \lesssim 15$ TeV, respectively.

On the other hand, the (flavor diagonal) operators \mathcal{O}_{ug} and \mathcal{O}_{dg} induce new chromo-magnetic dipole moment (CMDM) type, qqg and contact $qqgh$ interactions, which have a new Lorentz structure and, therefore, cannot be described by scaling the SM couplings. In particular, these new CMDM-like operators give rise to different Higgs + jet kinematics with respect to the SM. The effects of the light-quarks and b-quark CMDM-like effective operators, \mathcal{O}_{qg} ($q = u, d, c, s, b$), in Higgs production at the LHC was studied in [32, 62], where it was found that the inclusive Higgs production, $pp \rightarrow h + X$, and Higgs + b-jets events can be used to probe the CMDM-like interactions if its typical scale is $\Lambda_{qg} \sim$ few TeV. Here we will show that a better sensitivity to the scale of the effective quark CMDM-like operators, Λ_{qg} , can be achieved by analysing the exclusive $pp \rightarrow h + j(j_b) \rightarrow \gamma\gamma + j(j_b)$ Higgs production and decay channels and using the signal strength formalism with the cumulative cross-sections for a high $p_T^{cut} \sim 200 - 300$ GeV.

Note that, in the general case where the Wilson coefficients $f_{u\phi}$, $f_{d\phi}$, f_{ug} and f_{dg} are arbitrary 3×3 matrices in flavor space, the operators $\mathcal{O}_{u\phi}$, $\mathcal{O}_{d\phi}$, \mathcal{O}_{ug} and \mathcal{O}_{dg} will generate tree-level flavor-violating $u_i \rightarrow u_j$ and $d_i \rightarrow d_j$ transitions ($i, j = 1 - 3$ are flavor indices). One way to avoid that is to assume proportionality of these Wilson coefficients to the corresponding 3×3 Yukawa coupling matrices (Y_u and Y_d), in which case the field redefinitions which diagonalize the quark matrices also diagonalize these operators and the effective theory is automatically minimally-flavor-violating (MFV). That is,

$$\frac{f}{\Lambda^2} \mathcal{O}_{ug} \rightarrow Y_q \cdot \frac{f_{MFV}}{\Lambda_{MFV}^2} \mathcal{O}_{ug}, \quad (35)$$

so that the relation between generic NP parameters (f, Λ) and the corresponding parameters in the MFV effective theory is (for a single flavor q):

$$\frac{\Lambda_{MFV}^2}{\Lambda^2} = y_q \frac{f_{MFV}}{f}. \quad (36)$$

Thus, if $f_{MFV} \sim f$, then $\Lambda_{MFV} \sim \sqrt{y_q} \cdot \Lambda$, in which case $\Lambda_{MFV} \ll \Lambda$ for $q \neq t$. On the other hand, for $\sqrt{y_q} f_{MFV}/f \sim \mathcal{O}(1)$ we have $\Lambda_{MFV} \sim \Lambda$. In what follows we would like to keep our discussion as general as possible, not restricting to any assumption about the possible flavor structure of the Wilson coefficients. In particular, we will focus below on a single flavor (diagonal element) of these operators and assume that flavor violation is controlled by some underlying mechanism in the high-energy theory (not necessarily MFV), thereby suppressing the non-diagonal elements of these operators to an acceptable level.

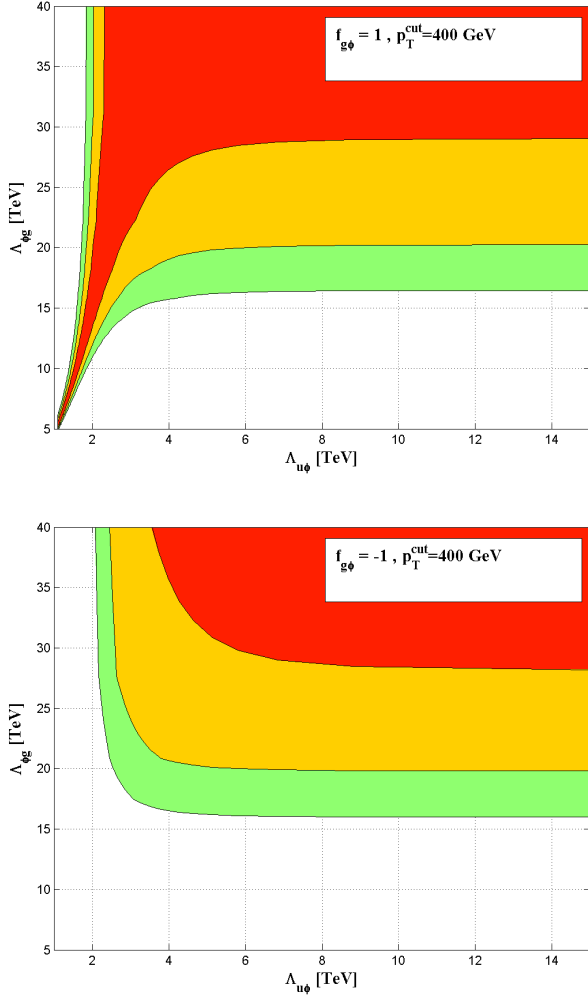


FIG. 9: The 68%(red), 95%(orange) and 99%(green) CL ranges in the $\Lambda_{q\phi} - \Lambda_{\phi g}$ plane, corresponding to $\Delta\mu_{hj}^f \equiv \left| \mu_{hj}^f - 1 \right| \leq 0.05, 0.1$ and 0.15 , respectively, with $p_T^{cut} = 400$ GeV and for $f_{\phi g} = 1$ (upper plot) and $f_{\phi g} = -1$ (lower plot). In both cases $|f_{u\phi}| = 1$, see text.

A. The case of Higgs + light-jet production

Let us consider first the operators $\mathcal{O}_{u\phi}$ and $\mathcal{O}_{\phi g}$, which, as seen from Eq. 34, modify the SM uuh and ggh couplings in a way that is equivalent to the kappa-framework (we will focus below only on the case of the 1st generation u-quark operator $\mathcal{O}_{u\phi}$).^[3] In particular, using Eq. 34 and the analysis performed in the previous section for NP

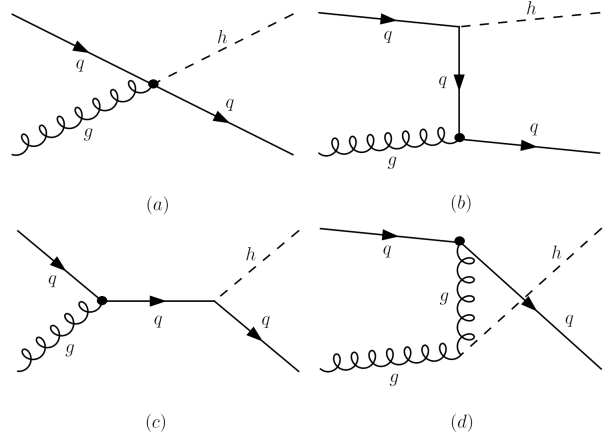


FIG. 10: Sample of tree-level diagrams for $gq \rightarrow hq$, $q = u, d, c, s, b$ generated by the CMDM-like effective operator \mathcal{O}_{qg} , where the heavy dot represents the CMDM-like vertices. There are additional diagrams for the subprocess $q\bar{q} \rightarrow hg$ and $g\bar{q} \rightarrow h\bar{q}$ that can also be obtained by crossing symmetry. In the case of a Higgs + light jet production, $pp \rightarrow h + j$, diagrams (b) and (c) are essentially absent (i.e., $y_q \rightarrow 0$).

in the kappa-framework, we plot in Fig. 9 the 68%, 95% and 99% CL sensitivity ranges in the $\Lambda_{u\phi} - \Lambda_{\phi g}$ plane, for $p_T^{cut} = 400$ GeV, assuming that $\mu_{hj}^f \sim 1 \pm 0.05(1\sigma)$. The sensitivity ranges are shown for the two cases $f_{\phi g} = \pm 1$, where in both cases we set $|f_{u\phi}| = 1$, since the cross-section $\propto \kappa_q^2$ (see Eq. 18) so that there is no dependence on the sign of $f_{u\phi}$ for $y_u^{SM}/y_b^{SM} \rightarrow 0$ (see Eq. 34).

We see that a measured value of μ_{hj}^f which is consistent with the SM at 3σ (i.e., with $0.85 \leq \mu_{hj}^f \leq 1.15$) will exclude NP with typical scales of $\Lambda_{\phi g} \lesssim 15$ TeV (equivalent to $\kappa_u \gtrsim 0.6$) and $\Lambda_{u\phi} \lesssim 2$ TeV (equivalent to $\kappa_g \gtrsim 1.1$), for $f_{\phi g} = -1$. In the case of $f_{\phi g} = 1$, there is an allowed narrow band in the $\Lambda_{u\phi} - \Lambda_{\phi g}$ plane, stretching down to NP scales of $\Lambda_{\phi g} \sim 5$ TeV and $\Lambda_{u\phi} \sim 1$ TeV, which are consistent with $0.85 \leq \mu_{hj}^f \leq 1.15$. We study next the effect of the CMDM-like operator \mathcal{O}_{ug} on $pp \rightarrow h + j$ (again focusing only on the u-quark operator). The tree-level diagrams corresponding to the contribution of \mathcal{O}_{ug} to $pp \rightarrow h + j$ are depicted in Fig. 10. They contain the momentum dependent CMDM-like uug vertex and $uugh$ contact interaction, which do not interfere with the SM diagrams in the limit of $m_u \rightarrow 0$. In particular, in the presence of \mathcal{O}_{ug} , the total $pp \rightarrow h + j$ cross-section can be written as:

$$\sigma^{hj} = \sigma_{SM}^{hj} + \left(\frac{f_{ug}}{\Lambda_{ug}^2} \right)^2 \sigma_{ug}^{hj}, \quad (37)$$

where the squared amplitudes for σ_{SM}^{hj} are given in Eqs. 6-8 (see also Eq. 17) and σ_{ug}^{hj} is the NP cross-section corresponding to the square of the CMDM-like amplitude, which is generated by the tree-level diagrams for $q\bar{q} \rightarrow gh$, $qq \rightarrow qh$ and $q\bar{q} \rightarrow qh$ shown in Fig. 10,

[3] The effects of $\mathcal{O}_{\phi g}$ and the top and bottom quarks operators $\mathcal{O}_{t\phi}$ and $\mathcal{O}_{b\phi}$ on the subprocess $gg \rightarrow hg$ were considered in [29], in the context of Higgs- p_T distribution in Higgs + jet production at the LHC.

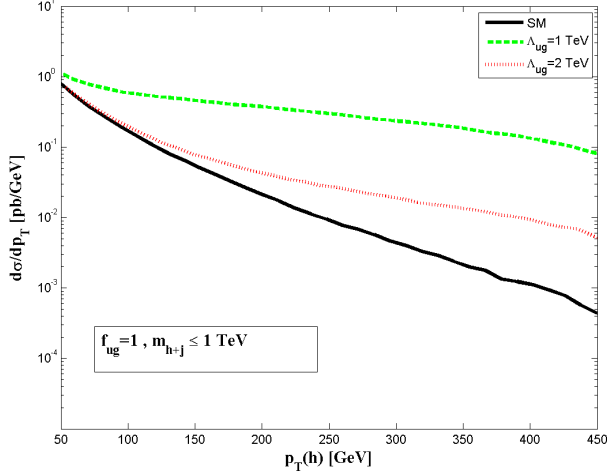


FIG. 11: The differential $p_T(h)$ distribution, $d\sigma(pp \rightarrow h + j)/dp_T(h)$, in the SM and with NP in the form of \mathcal{O}_{ug} , for $\Lambda_{ug} = 1$ and 2 TeV with $f_{ug} = 1$ and with an invariant mass cut of $m_{h+j} \leq 1$ TeV.

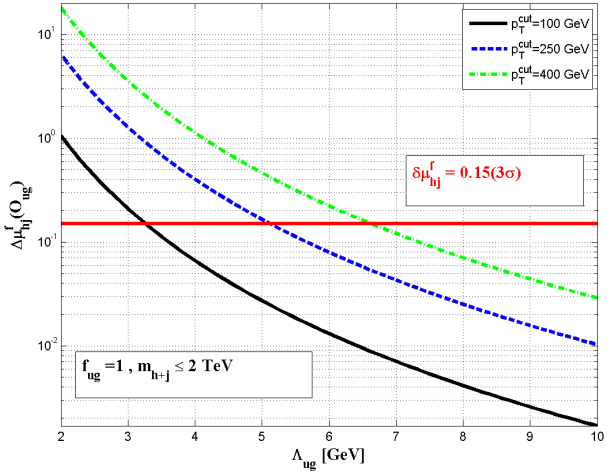


FIG. 12: The NP signal $\Delta\mu_{h,j}^f(\mathcal{O}_{ug})$, as a function of Λ_{ug} for $f_{ug} = 1$, $p_T^{cut} = 100, 250, 400$ GeV and an invariant mass cut of $m_{h+j} \leq 2$ TeV. The horizontal red line indicates the 5% accuracy level. See also text.

with an insertion of the effective CMDM-like uug and $uugh$ vertices. In particular, σ_{ug}^{hj} is composed of $\sigma_{ug}^{hj} = \sigma_{ug}^{hj}(q\bar{q} \rightarrow gh) + \sigma_{ug}^{hj}(qg \rightarrow qh) + \sigma_{ug}^{hj}(\bar{q}g \rightarrow \bar{q}h)$, where the corresponding amplitude squared (summed and averaged

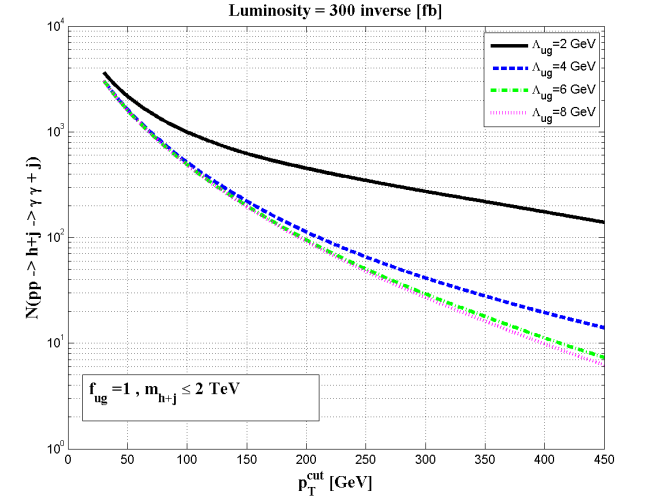
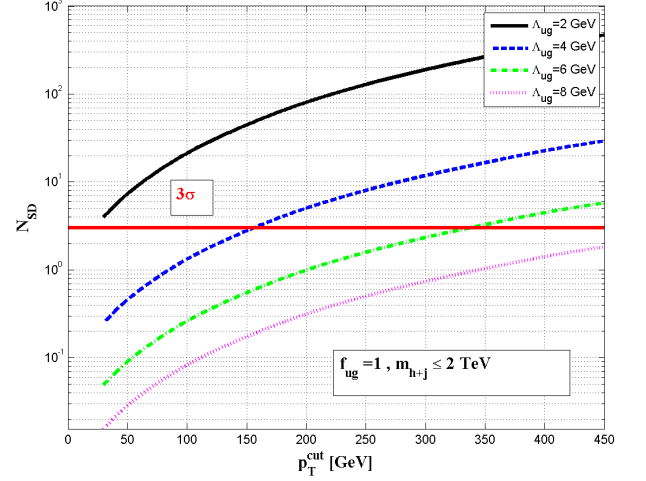


FIG. 13: The statistical significance of the signal (upper plot), $N_{SD} = \mu_{h,j}^f/\delta\mu_{h,j}^f$, for $\delta\mu_{h,j}^f = 0.05(1\sigma)$, and the expected number of $pp \rightarrow h + j \rightarrow \gamma\gamma + j$ events (lower plot), as a function of p_T^{cut} , for $\Lambda_{ug} = 2, 4, 6$ and 8 TeV with $f_{ug} = 1$ and with $\mathcal{L} = 300 \text{ fb}^{-1}$, a signal acceptance of 50% and an invariant mass cut of $m_{h+j} \leq 2$ TeV. See also text.

over spins and colors) are given by:

$$\sum \overline{|\mathcal{M}_{ug}^{q\bar{q} \rightarrow gh}|^2} = \frac{8}{C_{qq}} \hat{u} \hat{t} [1 - 4vC_g + 8v^2C_g^2], \quad (38)$$

$$\sum \overline{|\mathcal{M}_{ug}^{qg \rightarrow qh}|^2} = -\frac{C_{qq}}{C_{qq}} \sum \overline{|\mathcal{M}_{ug}^{q\bar{q} \rightarrow gh}|^2} (\hat{s} \leftrightarrow \hat{t}), \quad (39)$$

$$\sum \overline{|\mathcal{M}_{ug}^{\bar{q}g \rightarrow \bar{q}h}|^2} = -\frac{C_{qq}}{C_{qq}} \sum \overline{|\mathcal{M}_{ug}^{q\bar{q} \rightarrow gh}|^2} (\hat{s} \leftrightarrow \hat{u}), \quad (40)$$

with $\hat{s} = (p_1 + p_2)^2$, $\hat{t} = (p_1 + p_3)^2$ and $\hat{u} = (p_2 + p_3)^2$, defined for $q(-p_1) + \bar{q}(-p_2) \rightarrow h + g(p_3)$.

As illustrated in Fig. 11, the momentum dependent contribution from \mathcal{O}_{ug} drastically changes the $p_T(h)$ -dependence of the cross-section with respect to the SM

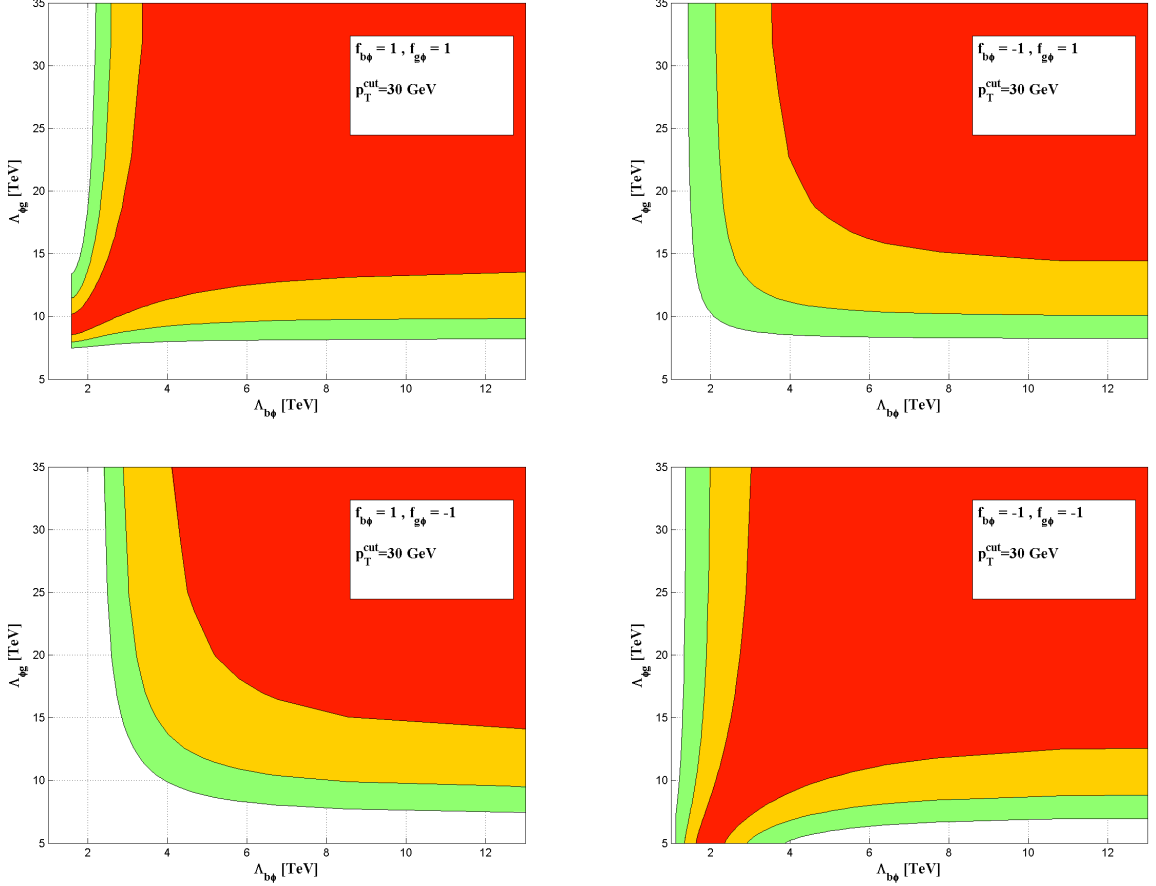


FIG. 14: The 68%(red), 95%(orange) and 99%(green) CL sensitivity ranges in the $\Lambda_{b\phi} - \Lambda_{\phi g}$ plane, corresponding to $\Delta\mu_{hj}^f \equiv \left| \mu_{hj}^f - 1 \right| \leq 0.05, 0.1$ and 0.15 , respectively, with $p_T^{cut} = 30$ GeV and for $f_{b\phi} = 1, f_{\phi g} = 1, f_{b\phi} = -1, f_{\phi g} = 1, f_{b\phi} = 1, f_{\phi g} = -1$ and $f_{b\phi} = -1, f_{\phi g} = -1$, as indicated in the figures.

and also with respect to the case where the NP is in the form of scaled couplings (i.e., in the kappa-framework). Indeed, the effect of \mathcal{O}_{ug} (or any other NP with a similar $p_T(h)$ behaviour) are better isolated in the harder Higgs p_T regime. This can be obtained by using a relatively high p_T^{cut} for the cumulative cross-section (see below).

Assuming no additional NP in the decay (the effects of \mathcal{O}_{ug} in the Higgs decay is $\propto (m_h/\Lambda_{ug})^4$ and is, therefore, negligible for $\Lambda \sim$ few TeV), the corresponding signal strength is:

$$\mu_{hj}^f(\mathcal{O}_{ug}) = 1 + \left(\frac{f_{ug}}{\Lambda_{ug}^2} \right)^2 R_{ug}^{hj}, \quad R_{ug}^{hj} \equiv \frac{\sigma_{ug}^{hj}}{\sigma_{SM}^{hj}}, \quad (41)$$

so that the NP signal, as defined in Eq. 12, is:

$$\Delta\mu_{hj}^f(\mathcal{O}_{ug}) = \left| \mu_{hj}^f(\mathcal{O}_{ug}) - 1 \right| = \left(\frac{f_{ug}}{\Lambda_{ug}^2} \right)^2 R_{ug}^{hj}. \quad (42)$$

In Fig. 12 we plot the NP signal, $\Delta\mu_{hj}^f(\mathcal{O}_{ug})$, as a function of Λ_{ug} with $f_{ug} = 1$, for p_T^{cut} values of 100, 250 and

400 GeV and an invariant mass cut $m_{h+j} \leq 2$ TeV. As expected (see Fig. 11), the sensitivity to Λ_{ug} is significantly improved the higher the p_T^{cut} is. In particular, while $\Delta\mu_{hj}^f/\mu_{hj}^f \gtrsim 5\%$ for $p_T^{cut} = 100$ GeV and $\Lambda_{ug} \lesssim 4$ TeV, for $p_T^{cut} = 400$ GeV we obtain $\Delta\mu_{hj}^f/\mu_{hj}^f \gtrsim 5\%$ for $\Lambda_{ug} \lesssim 8.5$ TeV.

In Fig. 13 we plot the statistical significance of the signal, $N_{SD} = \mu_{hj}^f/\delta\mu_{hj}^f$, for $\delta\mu_{hj}^f = 0.05(1\sigma)$, and the expected number of events, again assuming that the Higgs decays via $h \rightarrow \gamma\gamma$, i.e., $N(pp \rightarrow h + j \rightarrow \gamma\gamma + j)$, as a function of p_T^{cut} and for $\Lambda_{ug} = 2, 4, 6$ and 8 TeV with $f_{ug} = 1$ and an invariant mass cut $m_{h+j} \leq 2$ TeV. $N(pp \rightarrow h + j \rightarrow \gamma\gamma + j)$ is shown for an integrated luminosity of 300 fb^{-1} and a signal acceptance of 50%. We see, for example, that if $\Lambda_{ug} = 6$ TeV, then a high $p_T^{cut} \sim 350$ GeV is required in order to obtain a 3σ effect, for which $N(pp \rightarrow h + j \rightarrow \gamma\gamma + j) \sim \mathcal{O}(10)$ and $\mathcal{O}(100)$ is expected at the LHC with $\mathcal{L} = 300 \text{ fb}^{-1}$ and the HL-LHC with $\mathcal{L} = 3000 \text{ fb}^{-1}$, respectively.

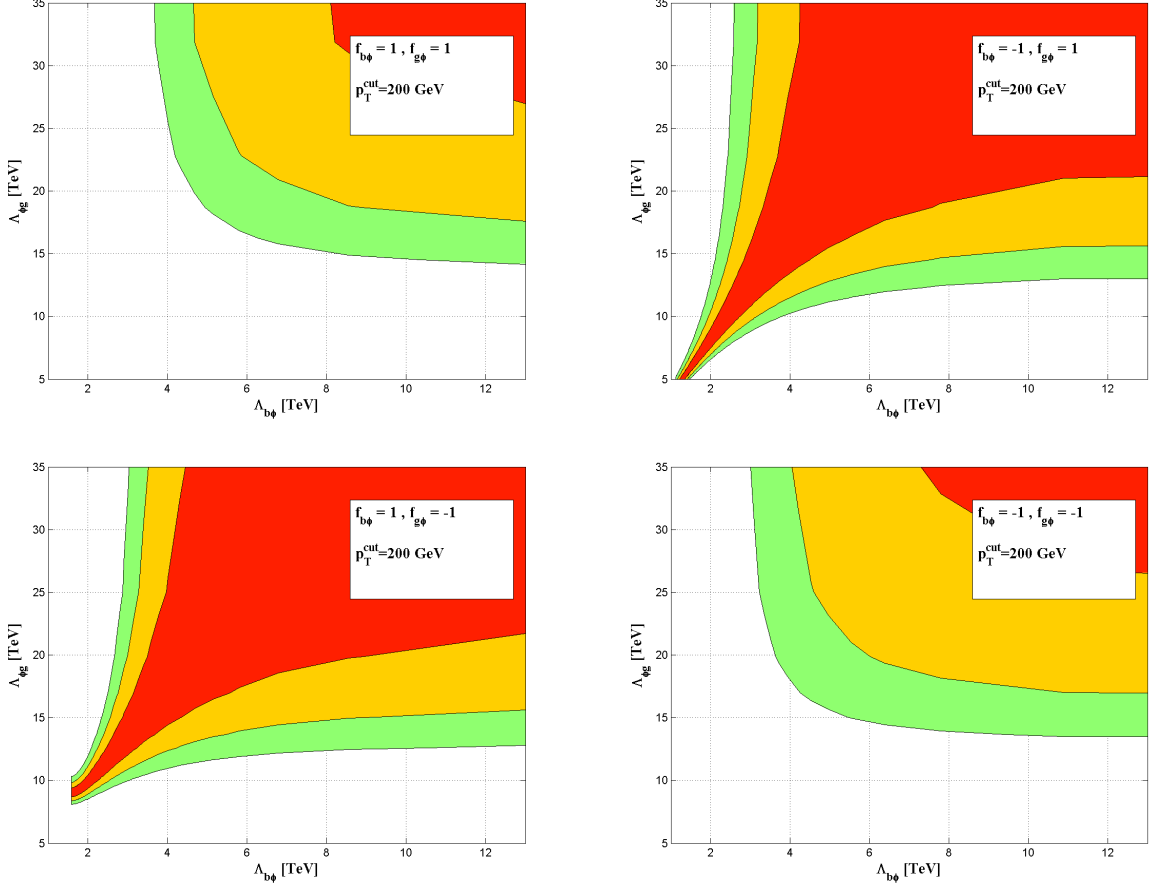


FIG. 15: Same as Fig. 14 for $p_T^{cut} = 200$ GeV.

B. The case of Higgs + b-jet production

As mentioned above, the effects of the NP operators $\mathcal{O}_{b\phi}$ and $\mathcal{O}_{\phi g}$ in $pp \rightarrow h + j_b$, can be described using the kappa-framework formalism of Eq. 15, with the NP factors multiplying the SM bbh Yukawa coupling (κ_b) and ggh coupling (κ_g) as prescribed in Eq. 34.

In Figs. 14 and 15 we plot the 68%, 95% and 99% CL sensitivity ranges in the $\lambda_{b\phi} - \Lambda_{\phi g}$ plane, for $(f_{b\phi}, f_{\phi g}) = (1, 1), (1, -1), (-1, 1), (-1, -1)$ and $p_T^{cut} = 30$ GeV and 200 GeV, assuming again that the signal strength had been measured to a 5%(1 σ) accuracy with a SM central value, i.e., $\mu_{h j}^f \sim 1 \pm 0.05(1\sigma)$. As in the kappa-framework analysis of the previous section, we use the two p_T^{cut} values, $p_T^{cut} = 30$ GeV and $p_T^{cut} = 200$ GeV, as two representative examples of a high and low statistics $pp \rightarrow h + j_b \rightarrow \gamma\gamma + j_b$ signal at the HL-LHC (see also Fig. 6). As expected, a better sensitivity to the NP is obtained for the higher $p_T^{cut} = 200$ GeV, where $\Lambda_{b\phi} \lesssim 3$ TeV and $\Lambda_{\phi g} \lesssim \mathcal{O}(10)$ TeV can be excluded at 3 σ if $\mu_{h j_b}^f$ is found to be consistent with the SM within 15% (3 σ).

Finally, we consider the case where the NP in $pp \rightarrow$

$h + j_b$ is due only to the b-quark CMDM-like operator \mathcal{O}_{bg} . The corresponding tree-level diagrams with the new momentum dependent CMDM-like bbg vertex and $bbgh$ contact interaction are shown in Fig. 10, where, as opposed to the $pp \rightarrow h + j$ case, here there is an interference (though small - see below) between the CMDM-like diagrams and the tree-level SM ones (depicted in Fig. 1). In particular, in the presence of \mathcal{O}_{bg} , the total $pp \rightarrow h + j_b$ cross-section can be written as:

$$\sigma^{h j_b} = \sigma_{SM}^{h j_b} + \frac{f_{bg}}{\Lambda_{bg}^2} \sigma_{bg}^{1, h j_b} + \left(\frac{f_{bg}}{\Lambda_{bg}^2} \right)^2 \sigma_{bg}^{2, h j_b}, \quad (43)$$

where $\sigma_{SM}^{h j_b}$ is the SM cross-section (the relevant SM squared amplitude terms are given in Eqs. 2,3,7,8) and the NP terms $\sigma_{bg}^{1,2}$ can be obtained from the following CMDM-like NP squared amplitudes (summed and aver-

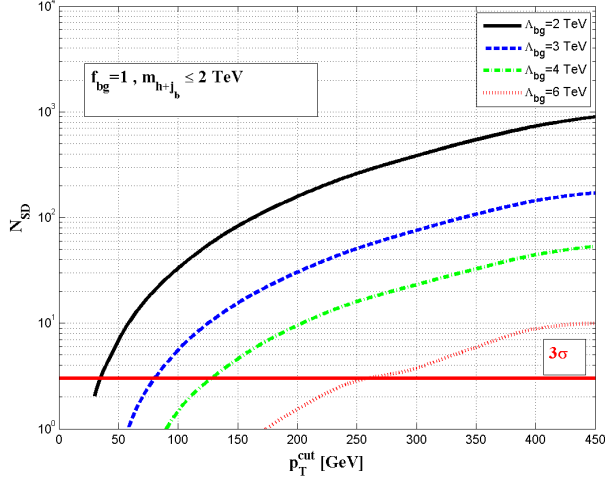


FIG. 16: The statistical significance of the signal, $N_{SD} = \mu_{h+j_b}^f / \delta\mu_{h+j_b}^f$, for $\delta\mu_{h+j_b}^f = 0.05(1\sigma)$, as a function of p_T^{cut} , in the presence of \mathcal{O}_{bg} (assuming no additional NP in the decay) for $f_{bg} = 1$ and $\Lambda_{bg} = 2, 3, 4$ and 6 TeV and with an invariant $h + j_b$ mass cut of $m_{h+j_b} \leq 2$ TeV.

aged over spins and colors):

$$\sum \left| \overline{\mathcal{M}_{bg}^{1,bg \rightarrow bh}} \right|^2 = \frac{8g_s y_b}{C_{qq}} (4vC_g \hat{t} - m_h^2), \quad (44)$$

$$\sum \left| \overline{\mathcal{M}_{bg}^{2,bg \rightarrow bh}} \right|^2 = -\frac{8}{C_{qq}} [\hat{s}\hat{u} (1 - 4vC_g + 8v^2C_g^2) + y_b^2 v^2 \hat{t}], \quad (45)$$

$$\sum \left| \overline{\mathcal{M}_{bg}^{1,\bar{b}g \rightarrow \bar{b}h}} \right|^2 = \sum \left| \overline{\mathcal{M}_{bg}^{1,bg \rightarrow bh}} \right|^2 (\hat{u} \leftrightarrow \hat{t}), \quad (46)$$

$$\sum \left| \overline{\mathcal{M}_{bg}^{2,\bar{b}g \rightarrow \bar{b}h}} \right|^2 = \sum \left| \overline{\mathcal{M}_{bg}^{2,bg \rightarrow bh}} \right|^2 (\hat{u} \leftrightarrow \hat{t}), \quad (47)$$

where again $\hat{s} = (p_1 + p_2)^2$, $\hat{t} = (p_1 + p_3)^2$ and $\hat{u} = (p_2 + p_3)^2$, defined for $b(-p_1) + \bar{b}(-p_2) \rightarrow h + g(p_3)$.

We see from Eqs. 44 and 46 above that the interference terms $\mathcal{M}_{bg}^{1,bg \rightarrow bh}$ and $\mathcal{M}_{bg}^{1,\bar{b}g \rightarrow \bar{b}h}$ (corresponding to σ_{bg}^{1,hj_b} in Eq. 43) are proportional to $y_b \sim \mathcal{O}(m_b/v)$ and are therefore sub-leading, so that the dependence of the $pp \rightarrow h + j_b$ cross-section on the sign of the CMDM-like Wilson coefficient, f_{bg} , is tenuous. As a result, σ^{hj_b} has a very similar p_T -behaviour as the one depicted in Fig. 11 for the $pp \rightarrow h + j$ case. In particular, here also, the Higgs p_T spectrum becomes appreciably harder with respect to the SM and also with respect to the case of the NP operators $\mathcal{O}_{b\phi}$ and $\mathcal{O}_{g\phi}$, due to the momentum-dependent σ_{bg}^{2,hj_b} term, which corresponds to the square of the b-quark CMDM-like diagrams, generated by the operator \mathcal{O}_{bg} and depicted in Fig. 10.

In Fig. 16 we plot the statistical significance of the \mathcal{O}_{bg} signal for $\delta\mu_{h+j_b}^f = 0.05(1\sigma)$, as a function of p_T^{cut} for $f_{bg} = 1$ and $\Lambda_{bg} = 2, 3, 4$ and 6 TeV, imposing an invariant

mass cut of $m_{h+j_b} \leq 2$ TeV. The results for $f_{bg} = -1$ are very similar due to the small interference between the CMDM-like and SM amplitudes (see discussion above). We see that, as expected, the sensitivity to the scale of the CMDM-like operator, Λ_{bg} , is higher the higher the p_T^{cut} is. We find, for example, that the effect of \mathcal{O}_{bg} with a typical scale of $\Lambda_{bg} \sim 4$ TeV can be probed in $pp \rightarrow h + j_b \rightarrow \gamma\gamma + j_b$ to the level of $N_{SD} \sim \mathcal{O}(10\sigma)$ with $p_T^{cut} = 200$ GeV. The expected number of $pp \rightarrow h + j_b \rightarrow \gamma\gamma + j_b$ events in this case (i.e., for $\Lambda_{bg} \sim 4$ TeV, $p_T^{cut} = 200$ GeV and an invariant mass cut of $m_{h+j_b} \leq 2$ TeV), assuming an integrated luminosity of 3000 fb^{-1} , a signal acceptance of $\mathcal{A} = 0.5$ and a b-jet tagging efficiency of 70%, $\epsilon_b = 0.7$, is $N(pp \rightarrow h + j_b \rightarrow \gamma\gamma + j_b) \sim 30$ (see also Fig. 6).

V. SUMMARY

We have examined the effects of various NP scenarios, which entail new forms of effective qqh and qqg interactions in conjunction with beyond the SM Higgs-gluon effective coupling, in exclusive Higgs + light-jet ($pp \rightarrow h + j$) and Higgs + b-jet ($pp \rightarrow h + j_b$) production at the LHC. We have defined the signal strength for $pp \rightarrow h + j(j_b)$ followed by the Higgs decay $h \rightarrow ff$, as the ratio of the corresponding NP and SM rates, and studied its dependence on the Higgs p_T spectrum. We specifically focused on $h \rightarrow \gamma\gamma$ and assumed that there is no NP in this decay channel.

We first analyse NP in $pp \rightarrow h + j(j_b) \rightarrow \gamma\gamma + j(j_b)$ within the kappa-framework, in which the SM Higgs couplings to the light-quarks (qqh) and to the gluons (ggh) are assumed to be scaled by a factor of κ_q and κ_g , respectively. In particular, in our notation the scale factors κ_q for all light-quark's Yukawa couplings ($q = u, d, c, s, b$) are normalized with respect to the b-quark Yukawa, $\kappa_q = y_q/y_b^{SM}$, so that in the SM we have e.g., $\kappa_b = 1$ and $\kappa_u \sim \mathcal{O}(10^{-3})$. This NP setup does not introduce any new Lorentz structure in the underlying hard processes (i.e., $gg \rightarrow gh, qq \rightarrow qh, \bar{q}q \rightarrow \bar{q}h, q\bar{q} \rightarrow gh$ in the case of $pp \rightarrow h + j$ and $bg \rightarrow bh, \bar{b}g \rightarrow \bar{b}h$ in the case of $pp \rightarrow h + j_b$), thus retaining the SM $pp \rightarrow h + j(j_b)$ kinematics. In particular, we find that strong bounds can be obtained in the $\kappa_g - \kappa_q$ plane at the LHC, by measuring a p_T -dependent signal strength for Higgs + jet events at relatively high Higgs p_T . For example, the combination of $\kappa_g < 0.8$ with $\kappa_u > 0.25$ ($\kappa_g < 0.8$ with $\kappa_b > 1.5$) can be excluded at more than 7σ at the HL-LHC with a luminosity of 3000 fb^{-1} , if the signal strength in the $pp \rightarrow h + j(j_b) \rightarrow \gamma\gamma + j(j_b)$ channels will be measured and known to an accuracy of 5%(1 σ), for high $p_T(h)$ events with $p_T(h) \geq 400(200)$ GeV. Recall that in our notation the corresponding SM strengths of these couplings are $\kappa_b = \kappa_g = 1$ and $\kappa_u \sim \mathcal{O}(10^{-3})$.

We also considered NP effects in $pp \rightarrow h + j(j_b)$ in the SMEFT framework, where higher dimensional effective operators modify the SM qqh Yukawa couplings and the Higgs-gluon ggh interaction by a scaling factor, similar

to the case of the kappa-framework for NP. We thus utilize an interesting “mapping” between the SMEFT and kappa-frameworks to derive new bounds on the typical scale of NP that underlies the SMEFT lagrangian. We find, for example, that $pp \rightarrow h + j(j_b) \rightarrow \gamma\gamma + j(j_b)$ events with high $p_T(h) > 400(200)$ GeV at the HL-LHC, are sensitive to the new effective operators that modify the qgh (Yukawa) and ggh couplings, if their typical scale (i.e., with $\mathcal{O}(1)$ dimensionless Wilson coefficients) is a few TeV and $\mathcal{O}(10)$ TeV, respectively.

Finally, as a counter example, we study the effects of NP in the form of dimension six u-quark and b-quark chromo magnetic dipole moment (CMDM)-like effective operators, which induce new derivative and new contact interactions that significantly distort the $pp \rightarrow h + j(j_b)$ SM kinematics and, therefore, cannot be described in

terms of scaled couplings. In particular, in this case, the high- p_T Higgs spectrum becomes significantly harder with respect to the SM. We thus show that $pp \rightarrow h + j(j_b) \rightarrow \gamma\gamma + j(j_b)$ events at the HL-LHC, with a high Higgs p_T of $p_T(h) \gtrsim 400(200)$ GeV, can probe the higher dimensional CMDM-like u-quark and b-quark effective operators, if their typical scale is around $\Lambda \sim 5$ TeV.

Acknowledgments: The work of AS was supported in part by the US DOE contract #DE-SC0012704.

-
- [1] G. Aad *et al.*, the ATLAS collaboration, JHEP **1409** (2014), 112, arXiv:1407.4222 [hep-ex].
- [2] G. Aad *et al.*, the ATLAS collaboration, Phys.Lett. **B738** (2014), 234, arXiv:1408.3226 [hep-ex].
- [3] G. Aad *et al.*, the ATLAS collaboration, Phys.Rev.Lett. **115** (2015) no.9, 091801, arXiv:1504.05833 [hep-ex].
- [4] G. Aad *et al.*, the ATLAS collaboration, JHEP **1608** (2016), 104, arXiv:1604.02997 [hep-ex].
- [5] V. Khachatryan *et al.*, the CMS collaboration, Eur.Phys. J. **C76** (2016), 13, arXiv:1508.07819 [hep-ex].
- [6] V. Khachatryan *et al.*, the CMS collaboration, arXiv:1606.01522 [hep-ex].
- [7] X. Chen, J. Cruz-Martinez, T. Gehrmann, E.W.N. Glover, M. Jaquier, JHEP **1610** (2016), 066, arXiv:1607.08817 [hep-ph].
- [8] R. Boughezal, F. Caola, K. Melnikov, F. Petriello, M. Schulze, JHEP **1306** (2013), 072, Phys.Rev.Lett. **115** (2015) no.8, 082003, arXiv:1504.07922 [hep-ph].
- [9] F. Caola, K. Melnikov, M. Schulze, JHEP **1306** (2013), 072, Phys.Rev. **D92** (2015) no.7, 074032, arXiv:1508.02684 [hep-ph].
- [10] X. Chen, T. Gehrmann, E.W.N. Glover, M. Jaquier, Phys.Lett. **B740** (2015), 147, arXiv:1408.5325 [hep-ph]; *ibid.* arXiv:1604.04085 [hep-ph].
- [11] R. Boughezal, C. Focke, W. Giele, X. Liu, F. Petriello, Phys.Lett. **B748** (2015), 5, arXiv:1505.03893 [hep-ph].
- [12] N. Greiner., S. Hoche, G. Luisoni., M. Schnherr, J.-C. Winter, JHEP **1701** (2017), 091, arXiv:1608.01195 [hep-ph].
- [13] R.V. Harlander, T. Neumann, K.J. Ozeren, M. Wiesemann, JHEP **1208** (2012), 139, arXiv:1206.0157 [hep-ph].
- [14] T. Neumann, C. Williams, Phys.Rev. **D95** (2017) no.1, 014004, arXiv:1609.00367 [hep-ph].
- [15] J.M. Lindert, K. Melnikov, L. Tancredi, C. Wever, arXiv:1703.03886 [hep-ph].
- [16] R.K. Ellis, I. Hinchliffe, M. Soldate, J.J. van der Bij, Nucl.Phys. **B297** (1988) 221.
- [17] U. Baur, E.W.Nigel Glover, Nucl.Phys. **B339** (1990), 38.
- [18] D. de Florian, M. Grazzini, Z. Kunszt, Phys.Rev.Lett. **82** (1999), 5209, hep-ph/9902483.
- [19] V. Ravindran, J. Smith, W.L. Van Neerven, Nucl.Phys. **B634** (2002), 247, hep-ph/0201114.
- [20] R. Boughezal, F. Caola, K. Melnikov, F. Petriello, M. Schulze, JHEP **1306** (2013), 072, arXiv:1302.6216 [hep-ph].
- [21] B. Jager, L. Reina, D. Wackerroth, Phys.Rev. **D93** (2016) no.1, 014030, arXiv:1509.05843 [hep-ph].
- [22] E. Braaten, H. Zhang, J.-W. Zhang, arXiv:1704.06620 [hep-ph].
- [23] O. Brein, W. Hollik, Phys.Rev. **D68** (2003), 095006, hep-ph/0305321.
- [24] S. Dittmaier, Michael Kramer, M. Spira, Phys.Rev. **D70** (2004), 074010, e-Print: hep-ph/0309204.
- [25] S. Dawson, C.B. Jackson, L. Reina, D. Wackerroth, Phys.Rev. **D69** (2004), 074027, e-Print: hep-ph/0311067; *ibid.* Phys.Rev.Lett. **94** (2005), 031802, e-Print: hep-ph/0408077; *ibid.* Mod.Phys.Lett. **A21** (2006), 89, e-Print: hep-ph/0508293.
- [26] J.M. Campbell *et al.*, e-Print: hep-ph/0405302.
- [27] A. Banfi, A. Martin, V. Sanz, JHEP **1408** (2014), 053, arXiv:1308.4771 [hep-ph].
- [28] C. Grojean, E. Salvioni, M. Schlaffer, A. Weiler, JHEP **1405** (2014), 022, arXiv:1312.3317 [hep-ph].
- [29] D. Ghosh, M. Wiebusch, Phys.Rev. **D91** (2015) no.3, 031701, arXiv:1411.2029 [hep-ph].
- [30] S. Dawson, I.M. Lewis, Mao Zeng, Phys.Rev. **D90** (2014) no.9, 093007, arXiv:1409.6299 [hep-ph].
- [31] R. V. Harlander, T. Neumann, Phys.Rev. **D88** (2013), 074015, arXiv:1308.2225 [hep-ph].
- [32] J. Bramante, A. Delgado, L. Lehman, A. Martin, Phys.Rev. **D93** (2016) no.5, 053001, arXiv:1410.3484 [hep-ph].
- [33] A. Azatov, A. Paul, JHEP **1401** (2014), 014, arXiv:1309.5273 [hep-ph].
- [34] M. Schlaffer, M. Spannowsky, M. Takeuchi, A. Weiler, C. Wymant, Eur.Phys. J. **C74** (2014) no.10, 3120, arXiv:1405.4295 [hep-ph].
- [35] M. Buschmann, C. Englert, D. Goncalves, T. Plehn, M. Spannowsky, Phys.Rev. **D90** (2014) no.1, 013010, arXiv:1405.7651 [hep-ph].
- [36] M. Grazzini., A. Inicka., M. Spira., M. Wiesemann, arXiv:1612.00283 [hep-ph].
- [37] A.L. Kagan, G. Perez, F. Petriello, Y. Soreq, S.

- Stoynev, J. Zupan, *Phys.Rev.Lett.* **114** (2015), 101802, arXiv:1406.1722 [hep-ph]; G. Perez, Y. Soreq, E. Stamou, K. Tobioka, *Phys.Rev.* **D92** (2015), 033016, arXiv:1503.00290 [hep-ph].
- [38] G. Perez, Y. Soreq, E. Stamou, K. Tobioka, arXiv:1505.06689 [hep-ph].
- [39] Y. Soreq, H.X. Zhu, J. Zupan, arXiv:1606.09621 [hep-ph].
- [40] F. Bishara, U. Haisch, P.F. Monni, E. Re, *Phys.Rev.Lett.* **118** (2017), 121801, arXiv:1606.09253 [hep-ph].
- [41] G. Bonner, H.E. Logan, arXiv:1608.04376 [hep-ph].
- [42] F. Yu, arXiv:1609.06592 [hep-ph].
- [43] L.M. Carpenter, T. Han, K. Hendricks, Z. Qian, N. Zhouc, *Phys.Rev.***D95** (2017) no.5, 053003, arXiv:1611.05463 [hep-ph].
- [44] J. Gao, arXiv:1608.01746 [hep-ph].
- [45] J.L. Diaz-Cruz, U.J. Saldaa-Salazar, *Nucl.Phys.* **B913** (2016), 942, arXiv:1405.0990 [hep-ph].
- [46] T. Han, X. Wang, arXiv:1704.00790 [hep-ph].
- [47] J. Alwall, R. Frederix, S. Frixione, V. Hirschi, F. Maltoni, O. Mattelaer, H.S. Shao, T. Stelzer, P. Torrielli, M. Zaro, *JHEP* **07** (2014), 079, arXiv:1405.0301 [hep-ph].
- [48] A. Alloul *et al.*, *Comput.Phys.Commun.* **185** (2014), 2250, arXiv:1310.1921 [hep-ph].
- [49] T. Hahn, S. Paehr, C. Schappacher, PoS LL2016 (2016) **068**, [J.Phys.Conf.Ser. **762** (2016) no.1, 012065], arXiv:1604.04611 [hep-ph].
- [50] Vladyslav Shtabovenko. *FeynCalc 9*. J. Phys. Conf. Ser., 762(1):012064, 2016 V. Shtabovenko, J.Phys.Conf.Ser. **762** (2016) no.1, 012064, arXiv:1604.06709 [hep-ph].
- [51] A.Martin, W. Stirling, R. Thorne, G. Watt, *Eur.Phys.J.* **C63** (2009), 189, arXiv:0901.0002 [hep-ph].
- [52] E. Conte, B. Fuks, G. Serret, *Comput.Phys.Commun.* **184** (2013) 222, arXiv:1206.1599 [hep-ph].
- [53] See e.g., Working Group Report: Higgs Boson, Sally Dawson *et al.*, arXiv:1310.8361 [hep-ex]; LHC Higgs Cross Section Working Group, S. Heinemeyer *et al.*, arXiv:1101.0593 [hep-ph], S. Dittmaier *et al.*, arXiv:1201.3084 [hep-ph], S. Heinemeyer *et al.*, arXiv:1307.1347 [hep-ph] and D. de Florian *et al.*, arXiv:1610.07922 [hep-ph].
- [54] LHC Higgs Cross Section Working Group Collaboration, A. David *et al.*, arXiv:1209.0040 [hep-ph].
- [55] C. Mariotti, G. Passarino, *Int.J.Mod.Phys.* **A32** (2017) no.04, 1730003, arXiv:1612.00269 [hep-ph].
- [56] M. Wiesemann, R. Frederix, S. Frixione, V. Hirschi, F. Maltoni, P. Torrielli, *JHEP* **1502** (2015), 132, arXiv:1409.5301 [hep-ph].
- [57] K.J. Ozeren, *JHEP* **1011** (2010), 084, arXiv:1010.2977 [hep-ph].
- [58] R. V. Harlander, K.J. Ozeren, M. Wiesemann, *Phys.Lett.* **B693** (2010), 269, arXiv:1007.5411 [hep-ph].
- [59] ATLAS and CMS Collaborations (G. Aad *et al.*), *JHEP* **1608** (2016), 045, arXiv:1606.02266 [hep-ex].
- [60] W. Buchmüller, D. Wyler, *Nucl. Phys.* **B268** (1986), 621; C. Arzt, M.B. Einhorn, J. Wudka, *Nucl. Phys.* **B433** (1995), 41; M. B Einhorn and J. Wudka, *Nucl. Phys.* **B876** (2013), 556.
- [61] B. Grzadkowski, M. Iskrzynski, M. Misiak, J. Rosiek, *JHEP* **1010** (2010), 085.
- [62] A. Hayreter, G. Valencia, *Phys.Rev.* D88 (2013), 034033, e-Print: arXiv:1304.6976 [hep-ph]; *ibid.*, arXiv:1411.0035 [hep-ph].